

Changing El Niño–Southern Oscillation in a warming climate

Cai Wenju^{1, 2, 3, *}, Santoso Agus^{3, 4, 5}, Collins Matthew⁶, Dewitte Boris^{7, 8, 9}, Karamperidou Christina¹⁰, Kug Jong-Seong¹¹, Lengaigne Matthieu¹², McPhaden Michael J.¹³, Stuecker Malte F.¹⁴, Taschetto Andréa S.^{4, 5}, Timmermann Axel^{15, 16}, Wu Lixin^{1, 2}, Yeh Sang-Wook¹⁷, Wang Guojian^{1, 2, 3}, Ng Benjamin³, Jia Fan¹⁸, Yang Yun¹⁹, Ying Jun^{20, 21}, Zheng Xiao-Tong^{1, 2}, Bayr Tobias²², Brown Josephine R.²³, Capotondi Antonietta^{24, 25}, Cobb Kim M.²⁶, Gan Bolan^{1, 2}, Geng Tao¹, Ham Yoo-Geun²⁷, Jin Fei-Fei¹⁰, Jo Hyun-Su²⁷, Li Xichen^{28, 29}, Lin Xiaopei^{1, 2}, McGregor Shayne³⁰, Park Jae-Heung¹¹, Stein Karl^{15, 16}, Yang Kai³¹, Zhang Li^{1, 2}, Zhong Wenxiu^{21, 32}

¹ Frontier Science Centre for Deep Ocean Multispheres and Earth System and Physical Oceanography Laboratory, Ocean University of China, Qingdao, China

² Qingdao National Laboratory for Marine Science and Technology (QNLN), Qingdao, China

³ Centre for Southern Hemisphere Oceans Research (CSHOR), CSIRO Oceans and Atmosphere, Hobart, TAS, Australia

⁴ Climate Change Research Centre (CCRC), University of New South Wales, Sydney, NSW, Australia

⁵ ARC Centre of Excellence for Climate Extremes, University of New South Wales, Sydney, NSW, Australia

⁶ College of Engineering, Mathematics and Physical Sciences, University of Exeter, Exeter, UK

⁷ Centro de Estudios Avanzados en Zonas Áridas (CEAZA), La Serena, Chile

⁸ Departamento de Biología Marina, Facultad de Ciencias del Mar, Universidad Católica del Norte, Coquimbo, Chile

⁹ Millennium Nucleus for Ecology and Sustainable Management of Oceanic Islands (ESMOI), Coquimbo, Chile

¹⁰ Department of Atmospheric Sciences, University of Hawai'i at Mānoa, Honolulu, HI, USA

¹¹ Division of Environmental Science & Engineering, Pohang University of Science and Technology (POSTECH), Pohang, South Korea

¹² MARBEC, Université Montpellier, CNRS, Ifremer, IRD, Sète, France

¹³ NOAA Pacific Marine Environmental Laboratory (PMEL), Seattle, WA, USA

¹⁴ Department of Oceanography and International Pacific Research Center, School of Ocean and Earth Science and Technology, University of Hawai'i at Mānoa, Honolulu, HI, USA

¹⁵ Center for Climate Physics, Institute for Basic Science (IBS), Busan, South Korea

¹⁶ Pusan National University, Busan, South Korea

¹⁷ Department of Marine Sciences and Convergent Technology, Hanyang University, Ansan, South Korea

¹⁸ CAS Key Laboratory of Ocean Circulation and Waves, Institute of Oceanology/Center for Ocean Mega-Science, Chinese Academy of Sciences, Qingdao, China

¹⁹ College of Global Change and Earth System Science, Beijing Normal University, Beijing, China

²⁰ State Key Laboratory of Satellite Ocean Environment Dynamics, Second Institute of Oceanography, Ministry of Natural Resources, Hangzhou, China

²¹ Southern Marine Science and Engineering Guangdong Laboratory (Zhuhai), Zhuhai, China

²² GEOMAR Helmholtz Centre for Ocean Research, Kiel, Germany

²³ School of Geography, Earth and Atmosphere Sciences, University of Melbourne, Parkville, VIC, Australia

²⁴ NOAA Physical Sciences Laboratory, Boulder, CO, USA

²⁵ Cooperative Institute for Research in Environmental Sciences, University of Colorado Boulder, Boulder, CO, USA

²⁶ School of Earth and Atmospheric Sciences, Georgia Institute of Technology, Atlanta, GA, USA

²⁷ Department of Oceanography, Chonnam National University, Gwangju, South Korea

²⁸ Institute of Atmospheric Physics, Chinese Academy of Sciences, Beijing, China

²⁹ University of Chinese Academy of Sciences, Beijing, China

³⁰ School of Earth, Atmosphere & Environment, Monash University, Clayton, VIC, Australia

³¹ State Key Laboratory of Numerical Modeling for Atmospheric Sciences and Geophysical Fluid Dynamics, Institute of Atmospheric Physics, Chinese Academy of Sciences, Beijing, China

³² School of Atmospheric Sciences and Guangdong Province Key Laboratory for Climate Change and Natural Disaster Studies, Sun Yat-sen University, Guangzhou, China

* Corresponding author : Wenju Cai email address : wenju.cai@csiro.au

Abstract :

Originating in the equatorial Pacific, the El Niño–Southern Oscillation (ENSO) has highly consequential global impacts, motivating the need to understand its responses to anthropogenic warming. In this Review, we synthesize advances in observed and projected changes of multiple aspects of ENSO, including the processes behind such changes. As in previous syntheses, there is an inter-model consensus of an increase in future ENSO rainfall variability. Now, however, it is apparent that models that best capture key ENSO dynamics also tend to project an increase in future ENSO sea surface temperature variability and, thereby, ENSO magnitude under greenhouse warming, as well as an eastward shift and intensification of ENSO-related atmospheric teleconnections — the Pacific–North American and Pacific–South American patterns. Such projected changes are consistent with palaeoclimate evidence of stronger ENSO variability since the 1950s compared with past centuries. The increase in ENSO variability, though underpinned by increased equatorial Pacific upper-ocean stratification, is strongly influenced by internal variability, raising issues about its quantifiability and detectability. Yet, ongoing coordinated community efforts and computational advances are enabling long-simulation, large-ensemble experiments and high-resolution modelling, offering encouraging prospects for alleviating model biases, incorporating fundamental dynamical processes and reducing uncertainties in projections.

78 **Key Points**

- 79 • Under greenhouse warming, majority of climate models project a faster background
80 warming in the eastern equatorial Pacific with an increase in ENSO rainfall variability.
81 This SST warming pattern continues for a century after global mean temperature
82 stabilises.
- 83
- 84 • ENSO rainfall response in the equatorial Pacific intensifies and shifts eastward,
85 leading to an eastward intensification of extratropical teleconnections.
- 86
- 87 • The observed equatorial Pacific surface warming pattern since 1980, though opposite
88 to the projected faster warming in the equatorial eastern Pacific, is within the inter-
89 model range in terms of SST gradients and is subject to influence from internal
90 variability.
- 91
- 92 • Variability of ENSO SST and extreme ENSO events are projected to increase under
93 greenhouse warming, with a stronger inter-model consensus in the latest generation of
94 climate models, but time of emergence for ENSO SST variability is later than that for
95 ENSO rainfall variability, opposite to that for mean SST versus mean rainfall.
- 96
- 97 • The future ENSO change is likely influenced by past variability, such that
98 quantification of future ENSO in the only realization of the real world is challenging.
- 99

- 100 • Although there is no definitive relationship of ENSO variability with the mean zonal
101 SST gradient or seasonal cycle, paleoclimate records suggest a causal connection
102 between vertical temperature stratification and ENSO strength, and a greater ENSO
103 strength since the 1950s than in past centuries, supporting an emerging increase in
104 ENSO variability under greenhouse warming.

105

106 El Niño-Southern Oscillation (ENSO), an alternation between warm phase El Niño and cold
107 phase La Niña events, is the most consequential year-to-year climate phenomenon on the
108 planet^{1,2,3}. During El Niño, as in the 2015-2016 extreme event^{4,5}, an anomalous warming in
109 the central and eastern equatorial Pacific weakens the west-minus-east zonal sea surface
110 temperature (SST) gradient along the equator. The associated weakening of the trade winds in
111 turn intensifies the warm anomaly, a process referred to as Bjerknes feedback⁶. Atmospheric
112 convection over the west Pacific moves eastward, resulting in global impacts that include
113 droughts and forest fires in countries bordering the western Pacific, but torrential rains and
114 floods in regions of the eastern equatorial Pacific^{1,2,3,7,8}. During a La Niña event, anomalously
115 low SST occurs in the central and eastern Pacific, convection over the western Pacific
116 intensifies and becomes more concentrated, and global impacts roughly opposite to those of
117 El Niño occur. ENSO's global reach affects agriculture, public health, infrastructure,
118 transportation, water security, ecosystems, and biodiversity^{1,2,3,9}.

119 Because of its widespread and consequential impacts, how ENSO may change in a warming
120 climate is one of the most compelling issues in climate change research today. A series of the
121 Intergovernmental Panel on Climate Change (IPCC) assessments^{10,11} have found that long-
122 term climatic conditions have changed, with historically high anthropogenic emissions of
123 greenhouse gases post 1990. Furthermore, there is no sign on the horizon that there will be an
124 abatement of these emissions, highlighting the urgency to understand ENSO's response to
125 greenhouse warming now and in the future^{12,13}.

126 Likely future ENSO changes and underpinning dynamics have been periodically
127 synthesized^{12,13} (**Fig. 1**). In a framework of ocean-atmosphere instability, in which ENSO is
128 sensitive to ocean-atmosphere coupling between equatorial trade winds and the west-minus-
129 east zonal SST gradient^{1,14,15,16}, a mean state change with weakened trade winds and a
130 reduced west-minus-east zonal SST gradient, as projected by most climate models^{12,13}, would
131 imply that ENSO would become more unstable¹⁶, therefore favoring greater amplitude under
132 global warming. However, from the 1990s, when climate models were first used to
133 investigate ENSO response to greenhouse forcing^{17,18}, to the fifth IPCC assessment report¹⁰,
134 climate models had shown no consensus on ENSO SST variability change in conventionally
135 defined regions in the central-eastern equatorial Pacific.

136 Instead, as synthesized in a 2015 review¹³, models that more realistically simulate
137 characteristics of extreme ENSO events tend to project systematic changes. These changes
138 include an increased frequency of El Niño events with extreme rainfall in the eastern

139 equatorial Pacific¹⁹⁻²², more frequent extreme equatorward swings of large-scale
140 convergence zones²³, a higher frequency of El Niño events featuring eastward propagating
141 SST anomalies²⁴, and a higher frequency of extreme La Niña events²⁵. The projected changes
142 are consistent with proxy records of ENSO variability suggesting that twentieth-century
143 ENSO activity is stronger than that during the previous centuries^{26,27,28}. A key development is
144 a realization that projection of the fundamental variable of ENSO SST variability should be
145 made at ENSO anomaly centres unique to each climate model²⁹. Meanwhile, advances
146 continue on our understanding of processes controlling the mean state changes³⁰⁻³³, ENSO's
147 interactions with variability in other ocean basins³⁴, and role of internal variability of the
148 climate system in the response of ENSO SST variability³⁵⁻³⁸. Although uncertainty remains,
149 an inter-model consensus on increased ENSO SST variability is emerging, with additional
150 support from models participating in the sixth phase of Coupled Model Intercomparison
151 Projects³⁹ (CMIP6).

152 In this review, we summarize the advances since 2015. We begin by describing ENSO event
153 diversity and asymmetry, changing ENSO in observations and proxy-data, and mean state
154 impacts on ENSO feedbacks. We subsequently discuss factors that contribute to the observed
155 and projected mean state changes. We continue by outlining the projected ENSO SST
156 variability change and associated mechanism, focusing on proposed mechanisms involving
157 mean state changes and other factors such as internal variability and inter-basin interactions
158 (**Fig. 1**). We then synthesize insight from paleo-proxy records in ENSO sensitivity to
159 external forcing. The review ends with identification of uncertainties and prospects for
160 improved quantification, detection, and high-resolution modelling of ENSO SST variability
161 change.

162

163 **ENSO in observations**

164 An important advance in ENSO research is the discovery that ENSO events are diverse and
165 their anomaly centres can be in the equatorial eastern Pacific (EP) or central Pacific (CP)^{8,40-}
166 ⁴⁴. Observed ENSO evolution and the associated feedbacks therefore need to be assessed in
167 terms of the diversity, as summarised in this section.

168 ***ENSO event diversity and asymmetry***

169 Strong El Niño events tend to peak in the EP, whereas strong La Niña and moderate El Niño
170 events tend to peak in the CP region, and La Niña events tend to be weaker than EP El Niño
171 events, and last for multiple years contributing to ENSO diversity and asymmetry^{5,42-45} (**Fig.**
172 **2, a-d**). The EP ENSO and CP ENSO can be approximated by spatially-fixed indices of SST
173 anomaly such as Niño3 (averaged SST anomaly over 5°S-5°N, 150°W-90°W) and Niño4
174 (5°S-5°N, 160°E-150°W), respectively, of which the combination is captured by the Niño3.4
175 (5°S-5°N, 170°W-120°W) index. The fundamental dynamics for ENSO diversity and
176 asymmetry is a nonlinear Bjerknes feedback, whereby after anomalous warming in the
177 eastern Pacific locally triggers atmospheric deep convection, zonal winds respond nonlinearly

178 with a greater response to additional warming. The nonlinear wind response leads to further
179 warming, resulting in an extreme EP El Niño, a process distinctively weaker in the central
180 Pacific^{44,46}. Heat discharge of the equatorial Pacific during strong El Niño cools the
181 equatorial Pacific subsurface conducive to development of La Niña. Mathematically, the
182 dynamics is reflected by a nonlinear relationship between the leading two Empirical
183 Orthogonal Functions of tropical Pacific SST variability such that their linear combination
184 represents EP and CP ENSO events, referred to as E-index and C-index^{29,46,47,48}. For
185 observations, time series of Niño3 and Niño4 can be approximately represented by E-index
186 and C-index (**Fig. 2a, b**), respectively.

187 *Observed ENSO changes*

188 ENSO has been changing. At the turn of the 21st century, there was a marked increase in
189 occurrences of CP El Niño events, which are weaker than EP El Niño events, contributing to
190 weaker ENSO SST variability⁴⁹. Since the 1970s, statistically significant changes have been
191 shown to occur in the evolution of El Niño and La Niña events from their embryonic to fully
192 mature stages⁵⁰, with both CP and EP ENSO events tending to originate from the western
193 Pacific, rather than the central and eastern Pacific before the 1970s⁵¹. Since late 1950s, CP
194 and EP ENSO variability has shown an increasing trend^{52,53,54}. Using data further back in
195 time, both EP-ENSO and CP-ENSO variability show an approximately 20% increase in the
196 post-1960 compared to the pre-1960 period (**Fig. 2a, b**), characterised by more frequent
197 extreme El Niño and extreme La Niña, respectively, with asymmetric spatial patterns (**Fig. 2c,**
198 **d**) and impact. However, there is uncertainty in data before the 1950s due to sparse
199 observations and sampling errors⁵⁵ which makes assessment of a potential impact of
200 greenhouse warming difficult.

201 Multiple paleo-ENSO proxy datasets do point to an approximately 25% intensification of
202 ENSO variability during the late 20th Century, relative to the pre-industrial period or
203 before^{26,27,28,56-59}. The intensification is supported by ENSO reconstructions that show greater
204 CP^{57,60} and EP⁵⁸ ENSO variability relative to the pre-industrial era. While these results imply
205 that anthropogenic greenhouse forcing might have already contributed to an increase in
206 ENSO variability, because these proxy records reflect both ENSO-related temperature and
207 rainfall variability, the extent of an increase in SST variability is unclear.

208 *ENSO feedbacks and mean state*

209 Observations since 1950 have identified ocean-atmosphere feedbacks responsible for ENSO
210 SST anomaly growth. During an El Niño, mean upwelling of cold water in the eastern
211 equatorial Pacific and the mean subsurface horizontal advection act to strengthen the
212 climatological horizontal and vertical SST gradients, and thus damp an initial warm SST
213 anomaly. In addition to this mean advective damping, the warm SST anomaly promotes deep
214 atmospheric convection and increasing tropical cloud amounts, consequently reducing
215 surface radiative and latent and sensible heat fluxes into the ocean, a process referred to as
216 thermal damping. On the other hand, the warm SST anomaly and the associated west-

217 minus-east SST gradient is reinforced by weakened equatorial trade winds through three
218 positive feedbacks^{12,61,62,63}: the Ekman feedback, in which the weakened trade winds reduce
219 upwelling of mean cold subsurface water in the eastern equatorial Pacific; the thermocline
220 feedback, whereby the weakened trade winds lead to a flattened thermocline with
221 anomalously warm subsurface water that is advected by mean upwelling to the surface; and
222 the zonal advective feedback, in which the weakened trade winds reduce the mean westward
223 oceanic transport of cold waters from the eastern Pacific. The relative importance of the
224 feedback processes differs across events. During a CP El Niño, for instance, the zonal
225 advective feedback tends to be more important than the thermocline feedback. Nonetheless,
226 the three positive feedbacks increase with the upper ocean stratification of the equatorial
227 Pacific^{29,64-67}.

228 Thus, the background climate state of the equatorial Pacific Ocean affects ENSO feedbacks
229 and ENSO intensity^{1,14,15,16}. Therefore, assessing ENSO response to greenhouse warming
230 requires an understanding of how the tropical Pacific mean state will change.

231

232 **Changes in mean state**

233 Based on ocean-atmosphere reanalyses^{68,69,70}, the observed mean state changes since 1980s,
234 in which emissions of greenhouse gases increase substantially, feature a strong strengthening
235 of the Walker circulation, west-minus-east SST gradient and equatorial easterly winds⁷¹⁻⁷⁴
236 (**Fig. 3a**). However, the simulated multi-model averaged changes by state-of-the-art climate
237 models over the same period are small (**Fig. 3b**), and the projected future mean state changes
238 are generally opposite to the observed since the 1980s (compare **Fig. 3a** and **Fig. 3c**). The
239 climate models, while continuing to show a persistent too-cold and too-west equatorial
240 Pacific cold-tongue bias (**Fig. 3d**), project a tropical Pacific future mean state change that
241 features a weakening of the Walker Circulation, a reduction of the equatorial west-minus-east
242 SST gradient, and an enhanced equatorial warming compared to off-equatorial regions^{12,13,75}
243 (**Fig. 3b**). Trends over the 1980-2019 period of the west-minus-east SST gradients in
244 individual models and in the reanalyses show that the observed changes since the 1980s are
245 within the inter-model range (**Fig. 3e**), before the long-term reductions in the west-minus-east
246 SST gradients in majority of models emerge (**Fig. 3f**). In this section, we outline processes
247 that contribute to the observed and projected future mean state changes, and their differences.

248

249 ***Forcing of the observed mean state changes since 1980***

250 The observed changes result from a balance of several processes including atmospheric
251 damping differential between the west and the east, an oceanic thermostat mechanism in the
252 east, internal variability on multidecadal scales, and inter-basin interactions. Most of these
253 processes contribute to the enhanced west-minus-east SST gradient.

254 **West-east damping differential.** The mean SST, and hence evaporative damping, is higher in
255 the western Pacific than in the east^{76,77,78}. In addition, the higher mean SST in the western
256 Pacific induces a greater net negative cloud-radiation feedback compared to the east⁷⁹. These
257 two processes are conducive to a reduced equatorial west-minus-east zonal SST gradient⁷⁸,
258 which in turn weakens equatorial easterly winds through Bjerknes feedback, leading to the
259 enhanced equatorial warming strongest in the east^{76,77}.

260 **Ocean thermostat.** On the other hand, assuming that the ocean is in quasi-equilibrium with
261 greenhouse gas forcing, these changes in atmospheric processes must be compensated by
262 changes in oceanic processes. Consistently, ocean upwelling in the equatorial eastern Pacific
263 can facilitate divergence of some of the added heat away from the eastern Pacific cold tongue
264 region, favouring less warming in the eastern than the western Pacific—an ocean thermostat
265 mechanism⁸⁰ also amplified by the Bjerknes feedback.

266 **Internal variability.** Multidecadal internal variability might also contribute to the observed
267 enhancement in the zonal SST gradient since 1980. However, limitations of *in situ*
268 observations and reanalyses have hindered an unambiguous attribution of the equatorial
269 Pacific trends since the 1980s to either natural or anthropogenic causes^{33,81}. For instance,
270 satellite-observed changes indicate a smaller strengthening of the Walker Circulation than
271 implied by reanalyses³³. While the satellite trend is still opposite to the simulated changes
272 averaged over large ensemble of model simulations, some ensemble members are also able to
273 reproduce the observed strengthening of the Walker Circulation³³ and the equatorial zonal
274 SST gradients⁸¹ (**Fig. 3e**), despite an overall underestimation of internal decadal variability in
275 models⁸². Thus, internal multi-decadal variability could be offsetting greenhouse warming-
276 induced changes and therefore leading to the observed trend since 1980s^{33,81,83}, which is,
277 therefore, likely transient in nature⁸¹.

278 **Inter-basin interactions.** Interactions with the two other tropical oceans on multi-decadal
279 timescales are shown to also play an important role in forcing the observed intensification of
280 zonal SST gradient since 1980 (REF.³⁴) (**Fig. 3a**). There has been faster warming in the
281 tropical Indian Ocean⁸⁴, Atlantic^{85,86}, or both^{87,88} since 1980, with anomalous atmospheric
282 sinking motion in the tropical Pacific conducive to an enhanced equatorial easterly surface
283 wind trend, and hence to a cooling in the eastern Pacific⁸⁵.

284 **Processes affecting projected future mean state changes**

285 For the projected long-term mean state changes, the competing processes between the
286 atmospheric damping differential and the oceanic thermostat mechanism also operate,
287 whereas multidecadal internal variability plays a diminishing role. Studies have found that
288 state-of-the-art climate models underestimate inter-basin interactions^{30,34,89,90,91}, which might
289 contribute to the long-term faster warming in the equatorial eastern Pacific than otherwise the
290 case³⁴. Additional factors that influence future mean state changes include impact from off-
291 equatorial Pacific Ocean warming, ENSO rectification, and the too-cold and too-west

292 equatorial Pacific cold tongue bias in climate models, though their relative importance is
293 unclear and likely model-dependent.

294 ***Off-equatorial Pacific warming.*** The equatorial Pacific mean state changes involve
295 processes outside the equatorial Pacific. The equatorial warming can partly be forced by
296 oceanic subduction of anomalous off-equatorial warming advected towards the equatorial
297 upwelling region, or a weakening of the Hadley circulation and wind-driven oceanic
298 subtropical overturning cells^{92,93}. Because of the multidecadal timescale involved in the off-
299 equatorial forcing, modelling studies suggest a mean state change with an initially
300 strengthened zonal SST gradient from the oceanic thermostat mechanism followed decades
301 later by a gradient weakening through oceanic subduction of anomalous off-equatorial
302 warming^{92,93,94}. This time-varying mean state change is supported by a modelling study
303 showing that models and ensemble members in a signal model that simulate historical
304 strengthening of the zonal SST gradient commonly exhibit a reversed future trend⁸¹.

305 ***ENSO rectification.*** While mean state changes such as the equatorial SST warming pattern
306 and enhanced stratification can change the balance of ENSO feedbacks and thereby ENSO
307 variability^{29,75,95}, ENSO variability change can rectify onto the mean state altering the
308 warming pattern in the tropical Pacific via nonlinear oceanic temperature advection^{96,97}. For
309 example, if extreme El Niño events become less frequent relative to La Niña events, a La
310 Niña-like mean state warming can emerge⁹⁶, although this is a case seen in only a small
311 number of models. In models with realistic nonlinear dynamical heating, that is, an
312 anomalous oceanic advection of temperature anomalies, or in models with realistic nonlinear
313 Bjerknes feedback, an increase in ENSO variability contributes to the emergence of an El
314 Niño-like warming pattern^{29,97}.

315 ***Cold tongue bias.*** Common present-day model biases within the tropical Pacific are
316 suggested to have contributed to a fast warming in the east in most climate models^{30,31,32}. For
317 example, the common too-cold and too-west cold tongue (**Fig. 3d**) might produce excessive
318 SST sensitivity to radiative warming in the cold tongue region, resulting in the erroneous
319 warming and weakening in west-minus-east SST gradient³². On the other hand, the cold
320 tongue bias can lead to an overestimated ocean thermostat mechanism under greenhouse
321 warming and spuriously weak shortwave radiation reduction in response to surface warming
322 in the central-to-western Pacific⁹⁸ such that alleviation of this bias would favour a faster
323 eastern Pacific warming than in the west⁹⁵. Despite the disparity between the observed
324 changes since 1980 and the projected future changes, the change might not be unidirectional
325 but time-varying. For example, the change in mean west-minus-east SST gradient could
326 initially be dominated by oceanic thermostat and subsequently by other processes leading to
327 opposite trends in late 21st century^{92,93,94}.

328 In terms of changes in the upper ocean temperature structure, ocean reanalyses over the 1910-
329 2017 period show an intensified equatorial Pacific upper-ocean stratification⁵¹. Although the
330 extent to which the intensified stratification is due to internal variability or greenhouse
331 warming is unclear, the increased stratification is consistent with the projected change for the

332 21st century when a transient increase in CO₂ continues¹³. The intensified stratification
333 underpins the projected increase in ENSO SST variability over the 21st century, as
334 summarised in the upcoming sections.

335

336 **Projected ENSO variability changes**

337 Climate model projections of ENSO SST change have generally been based on conventional
338 ENSO SST indices evaluated at fixed anomaly centres defined from observations^{12,13,35,99},
339 such as Niño3, without considering ENSO diversity. Projected changes in SST variability at
340 the fixed centre show no inter-model consensus. Much progress has occurred since the 90's
341 in understanding ENSO response to greenhouse forcing (see timeline in **Fig. 1**), including
342 that the lack of the inter-model consensus was in part due to competing changes between the
343 main ENSO linear positive and negative feedbacks despite robust change in individual
344 feedback term^{12,63,100,101,102} (**Fig. 1**, by 2010).

345 Robust changes emerged in key characteristics that underpin ENSO extremes^{19,21,24,25,75,103,104}
346 (**Fig. 1**, by 2015); for example, a doubling in frequency of El Niño events with extreme
347 rainfall impacts from about one event per 20 years in the century before 1990 to one event
348 per 10 years in the century after²¹. Such increasing frequency is also seen in CMIP6
349 models^{20,105}, and continues for as long as a century even after global mean temperature
350 stabilises at the warming target of the Paris Agreement, that is, 1.5-2.0°C warming relative to
351 the pre-industrial level^{22,106}.

352 Subsequently (by 2018, **Fig. 1**), emerging projection of enhanced ENSO SST variability was
353 found at anomaly centres unique to individual CMIP3 and CMIP5 models²⁹ in models with
354 more realistic ENSO diversity and nonlinearity, which are underestimated by most
355 models^{29,107,108}. The increase in ENSO SST variability is supported by CMIP6 models¹⁰⁹ with
356 a stronger inter-model consensus, as outlined below.

357 ***Increased ENSO SST variability***

358 The locations of ENSO SST anomaly centres can be different across models and from those
359 observed by as much as 30° longitude²⁹. Therefore, assessment of ENSO SST variability
360 change should consider CP and EP ENSO anomaly centres simulated in individual models,
361 and recent increased model agreement is partially due to correcting for model-specific
362 anomaly centres²⁹. Climate models tend to simulate a weaker distinction between EP and CP
363 events than observed²⁹. However, in CMIP5 models that reasonably simulate **the distinction**
364 **between** these two types of events, EP ENSO variance is projected to increase by
365 approximately 15% from the century before 2000 to the century after 2000 under 'business as
366 usual' emission scenario, with 88% of models producing an increase; CP ENSO variance is
367 also projected to increase, although the inter-model agreement is low²⁹ (59%). Similar
368 conclusions were found in an analysis of 11 CMIP6 models¹⁰⁹. A larger group of 23 CMIP6
369 models show an even stronger inter-model agreement, with all 23 models (100%) which

370 capture EP and CP events, generating an enhanced EP ENSO variance (**Fig. 4a**) and 65% of
371 the models generating an increase in CP ENSO variance (**Fig. 4b**). The stronger inter-model
372 agreement may be related to modest improvements in the simulated ENSO, such as pattern
373 and event diversity, and a slight reduction in the Pacific mean state biases^{110,111}. An overall
374 increase in climate sensitivity¹¹² might also be a factor. Even without model selection, the
375 majority of CMIP6 models generate an increase in Niño3 and Niño4 SST variability, with 28
376 and 27 out of 34 models, respectively, producing an increase of about 10-15% when
377 comparing variability over the 20th and 21st centuries.

378 The enhanced variability in EP and CP ENSO is associated with more occurrences of extreme
379 EP El Niño and extreme La Niña events²⁹ (**Fig. 4c, d**), increasing from 5.6 and 5.6 events per
380 century in the present-day to 8.9 and 8.3 events per century in the future climate, respectively.
381 In particular, dramatic swings from an extreme EP El Niño in a year to an extreme La Niña
382 the next year (**Fig. 4c, d**), as seen in 1997-1998, increase from 1.1 events per century in the
383 present day to 2.8 events per century in the future climate.

384 The implication of increased ENSO SST variability is expected to be greater than the changes
385 in teleconnection *per se* would suggest, due to the compounding effect of the mean state
386 change. In the presence of faster warming in the eastern equatorial Pacific Ocean than in the
387 surrounding regions, even weak El Niño events are able to induce strong atmospheric
388 convection^{13,21,64,104}. This would lead to extreme impacts via atmospheric teleconnection as
389 discussed next.

390 *Eastward intensification of teleconnections*

391 As a result of a projected faster warming in eastern equatorial Pacific under greenhouse
392 warming, the mean convection center shifts eastward during both CP and EP ENSO
393 events¹¹³⁻¹¹⁹, and the response of tropical eastern Pacific rainfall to ENSO strengthens^{19,20,21}
394 (**lower panels of Fig. 5, a-d**). In association, ENSO-induced Rossby wave trains, such as the
395 Pacific North America (PNA) and South Pacific America (PSA) teleconnection patterns, are
396 projected to shift eastward^{7,113-120} (**upper panels of Fig. 5, a-d**), despite uncertainties in early
397 generations of CMIP models^{121,122}. The large deepening/shallowing of the North Pacific
398 trough in the PNA teleconnection is likely to attain a stronger sensitivity to CP SST
399 anomalies than to EP SST anomalies under greenhouse warming¹¹⁶ (**Fig. 5c, d**).

400 These projected changes have important climatic implications for affected regions. For
401 example, as the ENSO-induced PNA pattern shifts eastward, El Niño-induced rainfall
402 anomalies are expected to intensify on the west coast of North America, and El Niño-induced
403 surface warming to expand eastward to occupy all of northern North America¹¹³. As a
404 consequence, many regions affected by ENSO in the present climate are likely to experience
405 more intense ENSO-driven rainfall variability in the future¹²³.

406 In addition, due to increased mean-state moisture and increased ENSO variability under
407 greenhouse warming, the asymmetric atmospheric response between El Niño and La Niña are
408 expected to increase^{115,120}. As a result, over many land areas, there will be a robust increase in

409 the spatial extent of ENSO teleconnections during austral summer in both temperature and
410 precipitation¹²⁴, leading to an increased impact in El Niño-induced droughts^{125,126}.
411 Furthermore, the projected increase in El Niño amplitude provides more favorable large-scale
412 conditions for tropical cyclone formation in the tropical Pacific^{127,128} such that island states,
413 such as Fiji, Vanuatu, Marshall Islands, and Hawaii, are likely to see a larger number of
414 tropical cyclones during El Niño events and reduced occurrences during La Niña events in
415 the future¹²⁸.

416

417 **Mechanism and processes influencing ENSO projection**

418 The increase in ENSO SST variability is underpinned by a stronger air-sea coupling arising
419 from an intensification of the equatorial Pacific upper-ocean stratification²⁹. The enhanced
420 stratification is caused by surface-intensified warming due to increasing greenhouse gas-
421 induced radiative forcing and freshening owing to increased precipitation, enhancing the
422 response of the surface mixed-layer to a given wind forcing^{29,64-67}. Thus, the projected
423 increase in ENSO SST variability is independent of faster warming in the eastern equatorial
424 Pacific than the west, a trend that underpins the projected increase in ENSO rainfall
425 variability²¹. Although models with stronger warming in the eastern equatorial Pacific do
426 tend to generate a greater increase in ENSO SST variability, and vice versa^{95,97,129}, the greater
427 warming can result from rectification of the increased ENSO SST variability onto the mean
428 state^{96,97}. Nevertheless, many factors affect the projection, such as interannual inter-basin
429 interactions, internal variability, and a too-cold equatorial Pacific cold tongue, as discussed
430 below.

431 ***Inter-basin interactions***

432 A strong appreciation has formed (**Fig. 1**, by 2019) that on interannual time scales, Atlantic
433 Niña with an anomalous cooling in the equatorial east Atlantic is conducive to a Pacific El
434 Niño^{130,131}, and an anomalous warming over the tropical North Atlantic may trigger a Pacific
435 La Niña¹³², whereas an Indian Ocean basin-wide warming can contribute to a transition from
436 El Niño to La Niña¹³³. The majority of models underestimate these remote impacts on
437 ENSO¹³⁴⁻¹³⁸, with implications on ENSO projections^{34,139}.

438 Under greenhouse warming, projected slower warming in the Atlantic Ocean than the Pacific,
439 due to a weakened oceanic heat transport from the South Atlantic induced by a weakened
440 Atlantic Meridional Overturning Circulation¹⁴⁰, can reduce the ability for Atlantic variability
441 to influence ENSO events, as convection is overall skewed toward the Pacific sector¹³⁶. In
442 addition, under greenhouse warming tropical North Atlantic SST anomalies decay faster due
443 to stronger thermal damping in a warmer climate¹³⁷, and tropospheric stability increases as
444 the lower atmosphere warms less than the upper troposphere¹³⁸, both acting to decrease the
445 forcing of Atlantic variability on ENSO. This scenario contrasts to what has occurred in the
446 post-1980 period, in which the Atlantic has exhibited rapid warming^{85,141} with more biennial
447 ENSO variability¹⁴².

448 Although there is no inter-model consensus on how interactions between ENSO and Indian
449 Ocean variability will change under greenhouse warming¹⁴³, the inter-basin warming
450 contrasts may vary with time, inducing non-unidirectional projected changes in ENSO, as
451 previously demonstrated in the case of a projected relative warming between the Pacific and
452 the Indian Ocean⁵³. However, the impact of the Atlantic and Indian Ocean future warming on
453 future ENSO is likely to be underestimated in climate models, because the simulated present-
454 day inter-basin interactions are underestimated^{30,34,85,89}.

455 *Internal variability*

456 It is also realised that ENSO projections are influenced by internal variability (**Fig. 1**, by
457 2020). ENSO variability and its future change differ vastly across ensemble members in a
458 single model under the same emission scenario due to internal variability, for example,
459 arising from small random perturbations to the same initial condition³⁵⁻³⁸. The inter-member
460 spread of future ENSO variability is not completely random, but dependent on past ENSO
461 behaviour: greater initial variability over a multi-decadal period being associated with smaller
462 future variability³⁵. Because of greater El Niño amplitude than that of La Niña, ocean-to-
463 atmosphere net heat loss during El Niño events is greater than heat gain during La Niña
464 events^{144,145}. The asymmetric heat flux results in a cumulative heat loss that is greater in
465 experiments with initially stronger ENSO variability, causing the thermocline to shoal in the
466 upper western Pacific and deepen in the eastern Pacific initially. Over time, the cumulative
467 heat loss leads to a cooling in the upper central and eastern equatorial Pacific. The cooling
468 partly offsets the greenhouse-forced upper-ocean stratification, such that initially strong
469 ENSO variability tends to be associated with future weak ENSO variability³⁵.

470 Such relationships are also seen in models with higher ENSO nonlinearity tending to project
471 weaker Niño3.4 variability and a reduced eastern equatorial Pacific warming⁴⁸. As
472 greenhouse gas concentrations increase further, the impact of internal variability relative to
473 the effect from greenhouse-induced change is expected to decrease, and uncertainty in the
474 projections is expected to be dominated by inter-model differences from the 2040's onward¹⁴¹.

475 *Impact from the cold-tongue bias*

476 Assessment of ENSO response mechanisms is affected by persistent model biases, of which
477 the common equatorial Pacific too-cold cold-tongue and too-west extension (**Fig. 3d**) is
478 suggested to have impact on ENSO simulation and projected ENSO changes¹⁴⁷. For instance,
479 the too-cold equatorial eastern Pacific cold tongue can lead to a spuriously weak Bjerknes
480 feedback that, despite being typically offset by a too-weak thermal damping^{148,149,150}, can
481 hamper simulation of realistic ENSO asymmetry⁹⁷ as warm anomalies are harder to grow to
482 establish atmospheric deep convection¹⁵⁰. While model selection based on realistic ENSO
483 asymmetry is used for ENSO projections, the asymmetry in selected models is still low
484 compared to the observed^{35,97}.

485 To summarise, although uncertainties remain, a scenario of increased ENSO SST variability
486 with more frequent ENSO SST extremes continues to emerge, with intensified ENSO

487 teleconnections. Thus, there are multiple lines of evidence indicating that ENSO can be
488 sensitive to climate change. Below we synthesize findings of ENSO sensitivity to past
489 climate change using proxy-based climate reconstructions to provide a historical perspective
490 of changing ENSO.

491

492 **Paleoclimatic context of ENSO changes**

493 Tropical Pacific interannual variability has been a feature of the Earth's climate system for
494 millions of years¹⁵¹. As such, assessments of forced changes in ENSO properties have been
495 carried out in the context of changes in Earth's orbit, volcanic eruptions, and greenhouse gas
496 forcing, as captured in both paleoclimate datasets, observational data, and climate models.
497 This section summarises new advancements of our understanding of ENSO response to past
498 climate forcings that might improve our understanding of its response to future anthropogenic
499 forcings, such as greenhouse gases and aerosols.

500 *Mean circulation and ENSO*

501 External paleoclimate forcings alter the mean state of the tropical Pacific, including the mean
502 surface temperature and its zonal and meridional gradients, surface wind patterns, the depth
503 of the thermocline, the magnitude of the annual cycle, and background noise. However,
504 comparison across periods finds no stable relationship in simulated climate between ENSO
505 variability and many mean circulation features. Since each past climate can be characterized by
506 multiple changes which can be coupled, it is often challenging to separate their role in influencing
507 ENSO variability in proxy records and model simulations alike.

508 Recent analysis of foraminifera from the eastern equatorial Pacific showed that in the
509 Pliocene weaker ENSO was associated with weaker zonal SST and vertical temperature
510 gradients¹⁵², in agreement with modelling studies^{153,154,155}. Last Glacial Maximum
511 reconstructions have corroborated the association of a weaker zonal SST gradient with
512 weaker ENSO variability¹⁵⁶, opposing interpretations from other proxy data that were
513 confounded by changes in the eastern Pacific seasonal SST cycle^{157,158,159}, as discussed in
514 REF.¹⁶⁰. Paleoclimate Model Intercomparison Project phase 3 and 4 (PMIP3 and PMIP4)
515 model experiments show no clear relationship between ENSO variance and zonal SST
516 gradient (**Fig. 6a, b**) or mean SST (**Fig. 6c**). The lack of a clear relationship is also true when
517 the climate system has not reached equilibrium, for example, last millennium simulations and
518 proxy synthesis¹⁶¹ show that models that best simulate modern tropical Pacific climate
519 frequently have a stronger ENSO SST variance when the west-minus-east mean SST contrast
520 is weaker, and vice versa, potentially as a result of ENSO rectification on the mean state^{162,163}.
521 However, there is vast diversity in the strength and direction of this relationship, suggesting
522 that it is not constant through time¹⁶⁴, and is likely controlled by multiple mechanisms¹⁶¹.

523 Reconstructed temperature variability at the equatorial Pacific during Last Glacial Maximum
524 and Pliocene suggests that ENSO strength is tied to the mean thermocline depth of the eastern
525 equatorial Pacific and the strength of the thermocline feedback^{152,156,165}. Modelling studies
526 support the idea that changes in ENSO variance during the mid- and early Holocene and

527 Pliocene can be attributed to the vertical ocean structure in the central and east equatorial
528 Pacific^{155,166,167,168}.

529 Overall, coupling of the zonal, meridional and vertical gradients, the lack of clear relationship
530 between changes in many mean circulation features and ENSO variability in paleoclimate
531 records and model experiments, and the fact that many of the available climate proxies
532 resolve equilibrium conditions rather than transient response to external forcings, make it
533 challenging to the use of any one of the past climates as analogues or reverse-analogue for
534 centennial-scale anthropogenic climate change.

535

536 *Orbital forcing and ENSO*

537 Changes in Earth's orbital characteristics modulate the seasonal amplitude of solar radiation,
538 generating changes in the mean climate and inducing seasonal shifts in temperature and
539 winds in the tropical Pacific, potentially influencing ENSO properties. General circulation
540 models forced with different orbital conditions simulate on average a 30-40% suppression of
541 the seasonal cycle amplitude of eastern tropical Pacific SST variability during the mid-
542 Holocene (6,000yrs ago) and a weak (10-20%) suppression of ENSO variability^{105,169}, but
543 large internal variability and inter-model spread challenge the robustness of these conclusions
544 (**Fig. 6a, d**). In the last interglacial, when orbital forcing was similar to that in mid-Holocene
545 forcing but stronger, models show a correspondingly larger decrease in ENSO variance (**Fig.**
546 **6a**) in agreement with limited coral records¹⁷⁰. The simulated orbital sensitivity of ENSO
547 stands in contrast to findings from paleoclimate reconstructions of ENSO variability, which
548 show intervals of reduced ENSO variance that are not in phase with orbital changes in
549 equatorial insolation^{166,171}. The simulated magnitude of the annual cycle in the last
550 interglacial is not distinguishable from historical simulations (**Fig. 6d**), challenging the notion
551 of a positive correlation between ENSO variance and annual cycle magnitude⁵⁹.

552 Spanning the last 7,000 years, ENSO proxy-based reconstructions show no clear orbitally
553 forced trend in ENSO variability since the mid-Holocene. Instead, there appears to be a
554 pronounced reduction in ENSO variability and the magnitude of the seasonal cycle between
555 3,000-5,000 years ago^{58,172}, a period which does not coincide with any known external
556 forcings. On the contrary, single foraminiferal records¹⁷³ and ENSO-related hydroclimate
557 proxy records from lakes and speleothems¹⁷⁴⁻¹⁷⁸ show significant changes in ENSO variance
558 under orbital forcing, in agreement with ENSO sensitivity to orbital forcing in paleoclimate
559 model experiments but several times of magnitude higher than the changes found in these
560 experiments, sometimes of opposite direction⁵⁹.

561 Some of the model-proxy discrepancies can be reconciled by considering changes in ENSO
562 flavours and their different teleconnection patterns^{167,179}. For example, the mid-Holocene
563 ENSO reduction was most pronounced in the eastern equatorial Pacific, whereas CP ENSO
564 events remained relatively unaffected or even slightly increased¹⁶⁷. Given the model
565 uncertainties as well as the discrepancy between paleo-climate reconstructions and model

566 simulations, it appears that ENSO's sensitivity to orbital forcing remains highly uncertain⁵⁹.

567 ***Volcanic forcing and ENSO***

568 The impact of strong volcanic forcing on ENSO variability in the past also remains an open
569 question; an answer to this question can improve our understanding of the role of natural and
570 anthropogenic aerosols in ENSO variability in present and future climates¹⁸⁰. Some model
571 and proxy studies suggest an increase in the probability of El Niño events in the year
572 following an eruption^{27,181-185}, whereas others show a weak La Niña response^{186,187}, or no
573 clear response^{188,189,190}. Multiple factors are involved, including the Pacific-wide initial
574 conditions, and the location and season of the eruption and the spatial structure of the
575 volcanic aerosols¹⁹¹⁻¹⁹⁵. For example, the impact of tropical eruptions on ENSO is modelled
576 to enact via movement of the inter-tropical convergence zone and extratropical
577 teleconnections and northern hemisphere tropical eruptions generate an El Niño-like response.
578 Conversely, southern hemisphere tropical eruptions induce a La Niña-like response¹⁹⁴, as
579 does a uniform negative radiative forcing over the tropics contrary to the expectation from the
580 ocean dynamical thermostat mechanism⁸⁰. Thus, reducing proxy dating uncertainties and
581 accounting for the latitude and timing of eruptions is important for assessing ENSO's
582 sensitivity to aerosol forcing.

583 In summary, given the short length of the instrumental record, paleoclimate reconstructions
584 and model experiments are critical for understanding ENSO response to external climate
585 forcing, especially in the context of the sensitivity of ENSO feedbacks to changes in the mean
586 state^{105,167}. In particular, paleoclimate records appear to show a causal connection between
587 the equatorial Pacific vertical temperature stratification and ENSO strength. However,
588 limitations of paleoclimate records exist⁵⁹, arising from many factors including nonlinearities
589 and non-stationarity in teleconnected proxy records¹⁹⁶, subsampling natural ENSO
590 variability, and difficulty in separating the impacts of ENSO, its diversity and seasonal cycle
591 changes in both direct and teleconnected/indirect ENSO proxies. Further, most of these proxy
592 records reflect ENSO-related temperature, rainfall and salinity, which can lead to
593 nonlinearities and non-stationarity in the recorded signal¹⁹⁶. In addition, regional topography
594 and mesoscale circulation processes can lead to departure of regional signals from the
595 expected large-scale signature of ENSO events¹⁹⁷. Thus, the observed interannual variance in
596 land-based hydroclimate or coral-based records likely reflect a change in ENSO-related
597 temperature and hydrological variability combined, ENSO diversity and the regional or large-
598 scale teleconnections^{167,179,198}. Despite the limitations, paleoclimate reconstructions, when
599 carefully combined with dynamical understanding, offer the ability to groundtruth model
600 simulations and to inform targeted experiments for distinguishing underlying mechanisms.

601

602 **Conclusions, uncertainties, and prospects**

603 There is an emerging inter-model consensus among models capturing the distinction between
604 EP and CP ENSO events, stronger in CMIP6 than CMIP5, that ENSO SST variability at the

605 unique centres in each model is likely to increase, leading to an increase in frequency of
606 extreme El Niño and extreme La Niña events in terms of SST anomaly magnitude.
607 Associated with the increase in ENSO SST variability, the equatorial Pacific rainfall response
608 to ENSO intensifies and shifts eastward, as do extratropical teleconnections, leading to
609 stronger climate impacts in the future. There are also increasing lines of paleoclimatic
610 evidence that ENSO variability has increased since the 1950s compared with past centuries,
611 and that ENSO variability strength on long timescales increases with the equatorial Pacific
612 vertical temperature gradient, consistent with the emerging consensus on increased ENSO
613 variability under greenhouse warming. In addition, future changes in ENSO SST are not
614 simply a function of emission scenarios but are influenced by the past history of ENSO
615 variability.

616 However, uncertainties remain. On multi-decadal timescales, the disparity between the
617 projected weakening in west-minus-east zonal SST gradient and the observed strengthening
618 over the past several decades^{31,32,33,81}, the too-west and too-cold equatorial Pacific cold
619 tongue, and the too-weak inter-basin interactions^{30,34,89,90}, reduce confidence in the projected
620 change. On interannual time scales, simulated inter-basin teleconnections are also too weak,
621 leading to a weaker ENSO impact on the Atlantic Niño/Niña, tropical North Atlantic and
622 Indian Ocean SST variability; in turn, their feedbacks on ENSO are too weak^{135,137,138}. It is
623 not clear how these two-way interactions will change and how the changes will affect ENSO.

624 Further, ENSO is coupled with and influenced by other variability at higher latitudes of the
625 Pacific. For example, El Niño events are preceded by and coupled with warm anomalies of
626 the North Pacific meridional mode^{199,200,201} and forced by southerly jets from southwestern
627 Pacific²⁰². We have incomplete knowledge of how these tropical-extratropical connections
628 are simulated in climate models and how they will respond to greenhouse warming.

629 In terms of ENSO properties, we know little about how other essential characteristics of
630 ENSO may change, such as the termination and onset of ENSO events, coupling between
631 stochastic noise and ENSO, and interactions between ENSO and the annual cycle^{13,59}. In
632 terms of ENSO physics, the role of eddy-induced oceanic heat transport and oceanic turbulent
633 mixing is not well understood or parameterised²⁰³, nor are sub-grid atmosphere process such
634 as atmospheric convection, cloud formation and their coupling to other ENSO processes²⁰⁴.

635 Nevertheless, coordinated community efforts like CMIP and advances in computational
636 power will continue to facilitate progress. Large-ensemble simulations²⁰⁵, long control
637 climate simulations, and high-resolution climate modelling (e.g., 0.1° in horizontal resolution
638 for the ocean model component) show great promise in addressing key questions about
639 ENSO in a warmer world, example of which we highlight further below.

640 When the “signal” of increased ENSO SST variability or the changing mean state may clearly
641 emerge from the background noise of internal variability, or whether such a signal will ever
642 be detectable in a single realization of the real world, is an open question that is largely
643 unexplored. Long multi-century control simulations of the climate system provide a wide
644 range of realizations for this assessment. The concept of the ‘Time of Emergence’ for SST
645 and precipitation signals in the equatorial Pacific, referenced to pre-industrial conditions,
646 indicate when it should be possible to detect these signals against the background noise of
647 natural internal variability²⁰⁶. For changes in mean SST in Niño3.4 region under the most
648 aggressive greenhouse gas emission scenario, the time of emergence should have been

649 around the turn of the 21st century (**Fig. 7a**). However, the discrepancy between models and
650 observations and the inter-model spread mean that we have not been able to conclude with
651 confidence that we have observed a clear greenhouse gas forced mean-state temperature
652 change. For changes in mean precipitation in the Niño3.4 region, the signal may not emerge
653 until mid-21st century. Conversely, however, the situation for SST and precipitation
654 variability is reversed, with the rainfall variability emerging sooner than the SST variability
655 (**Fig. 7b**). The earlier emergence of rainfall variability confirms the robust signal of more
656 extreme El Niño events in the future when measured by a rainfall threshold²¹. These results
657 suggest that ENSO changes should be detectable within the 21st century; however, the time of
658 emergence for teleconnections impacting ENSO-affected regions awaits investigation.

659 Large ensemble experiments within a single model have led to a realization that internal
660 variability^{36,37} and butterfly effect influence projected ENSO change. Available simulations
661 suggest that while responding to greenhouse warming, ENSO constantly self-regulates in
662 accordance with its own past behaviour. That is, high past variability takes heat out of the
663 upper equatorial Pacific Ocean, off-setting greenhouse warming-induced upper ocean
664 stratification and weakening ENSO's response, which in turn sets up for a strong subsequent
665 response by reducing oceanic heat loss³⁵. The self-regulation raises an issue of whether there
666 is a deterministic equilibrium ENSO response to greenhouse warming in a single realization.
667 In other words, is ENSO change quantifiable in a given window of time in the future? Large
668 ensemble experiments with multiple models offer an opportunity to test the robustness of this
669 self-regulating behaviour and to inspire theoretical models of the associated process.

670 Furthermore, high resolution climate models not only better resolve ENSO teleconnection
671 patterns, intensity and associated climate extremes at regional scales, subgrid ocean and
672 atmosphere process, but also allow explicit definition of previously unresolved physical
673 processes. One example is heat transport induced by equatorial Pacific oceanic eddies (such
674 as tropical instability waves) on the mean state heat balance of the equatorial Pacific. For the
675 equatorial Pacific mean state, eddy-induced heat transport represents a substantial heat source
676 comparable to heat uptake from the atmosphere²⁰⁷. The eddy-induced heat source is reduced
677 during El Niño but increases during La Niña, constraining ENSO amplitude²⁰⁸ while
678 substantially contributing to ENSO irregularity and predictability²⁰³. Given that such eddy
679 effects are not resolved by low-resolution climate models, it is likely that the simulated cold
680 tongue bias²⁰⁹ and other ENSO property biases¹⁴⁸ in CMIP models could be in part due to the
681 absence of the eddy process. Thus, high-resolution ENSO modelling offers a path forward for
682 substantial improvement in ENSO simulations and projections.

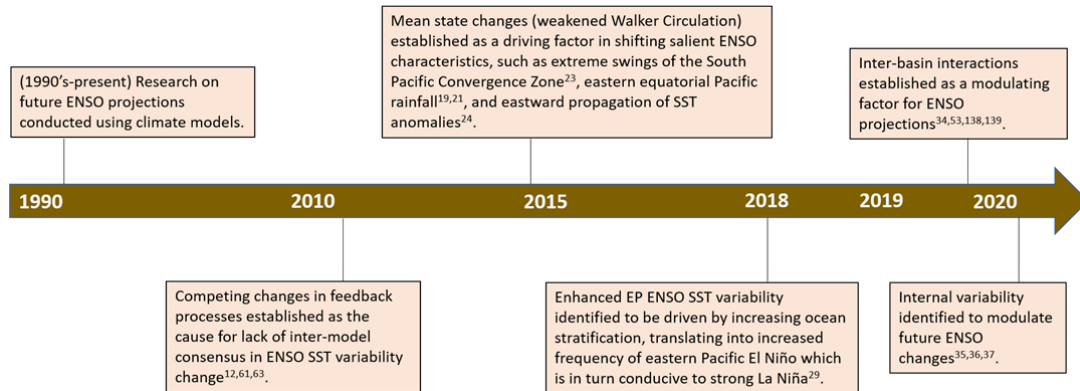
683 To conclude, despite rapid progress over the past five years the issue of ENSO response to
684 greenhouse warming is far from resolved, and many fundamental questions remain. The
685 coming decade offers opportunities for substantial advances as community efforts strengthen,
686 cutting-edge ideas emerge, and realistic models become available. The robust scientific
687 process, whereby debates inspire research and progress identifies new issues, will propel the
688 field forward.

689

690

691 **Figures and captions**

692



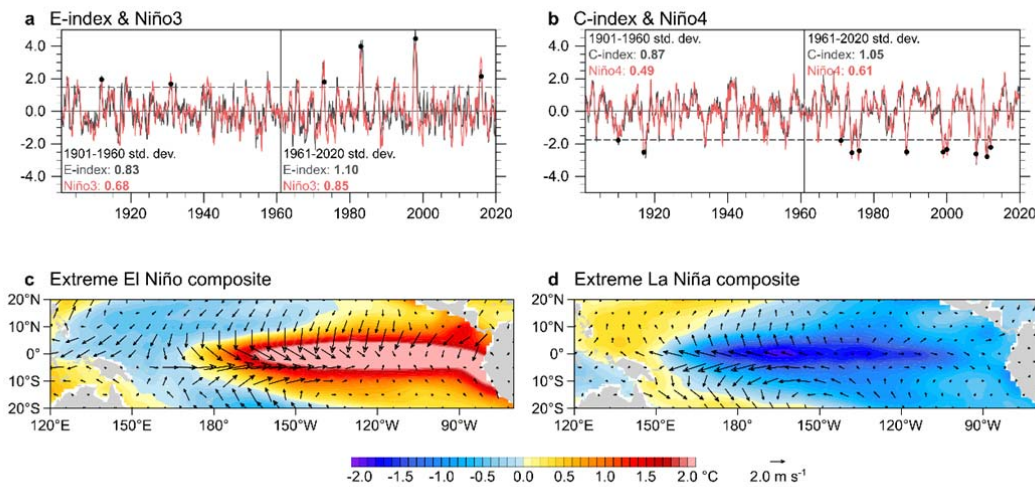
693

694

695 **Figure 1 | Timeline of development in understanding ENSO response to greenhouse forcing.**

696 Each development is marked at an approximate time and is a result of studies and multiyear-long
 697 effort starting in the 90's when climate models were first used to study ENSO future projections^{17,18}.

698



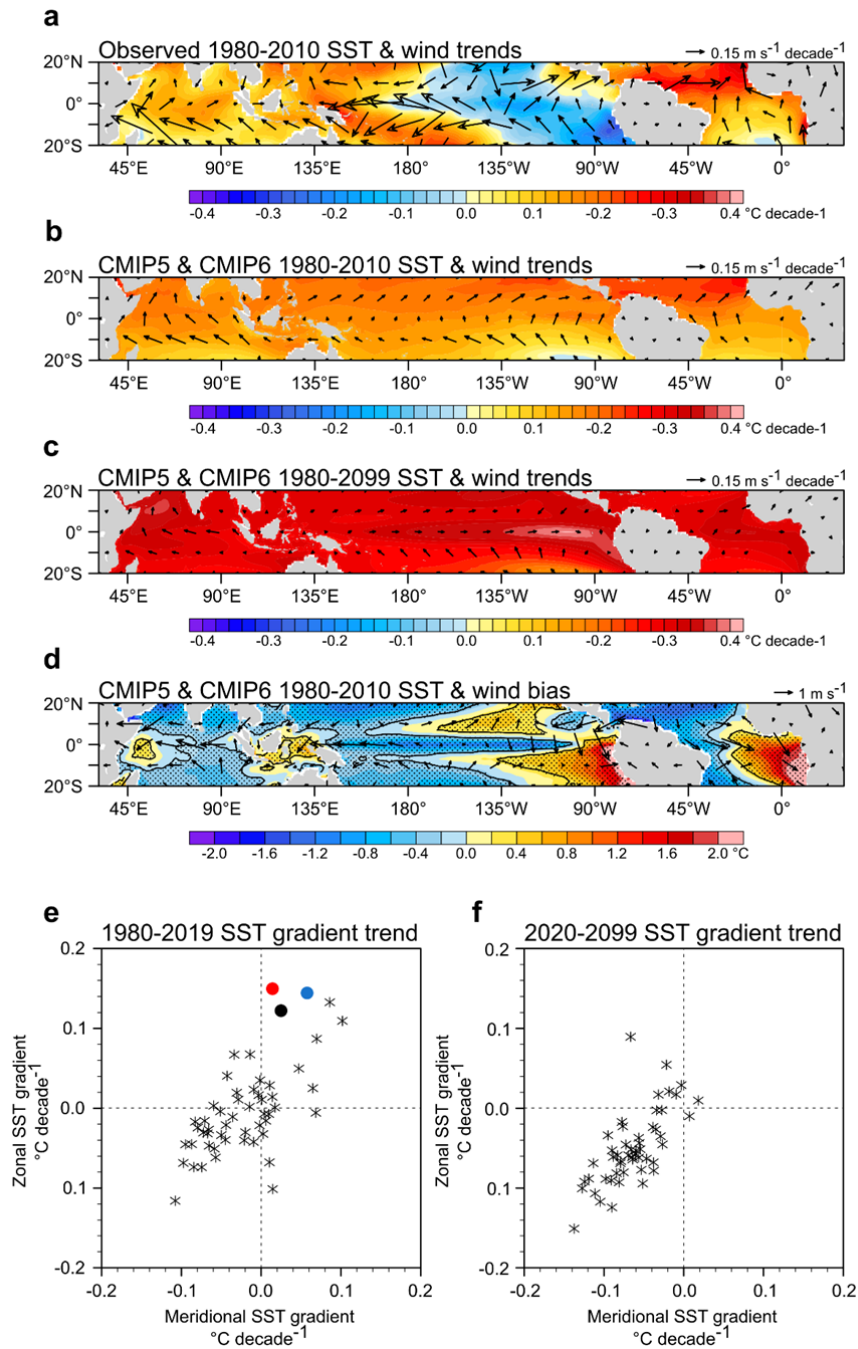
699

700

701 **Figure 2 | Observed normalized Niño3 and Niño4 indices and their representation using**

702 **E-index and C-index.** Shown are based on average across three products^{68,69,70} from 1901 to
 703 2017. a, b, Niño3 and Niño4 timeseries plotted with E-index and C-index for EP-ENSO and
 704 CP-ENSO, respectively. The numbers in each panel indicate the standard deviations of the
 705 indices, with the numbers representing the 1901-1960 and 1961-2017 periods. c, d, SST and
 706 surface wind composite anomalies for extreme El Niño events defined as when DJF mean E-
 707 index >1.5 s.d. (black dots in a), and for extreme La Niña defined as when DJF mean C-index

708 < -1.75 s.d. (black dots in b), respectively. Anomaly centres for extreme El Niño and extreme
 709 La Niña are in the eastern and central equatorial Pacific, respectively. Increased variability of
 710 Niño3 or E-index in the post-1960 period is characterised by an increased frequency of
 711 extreme El Niño, and increased variability in Niño4 or C-index in the post-1960 period is
 712 characterised by an increased frequency of extreme La Niña.



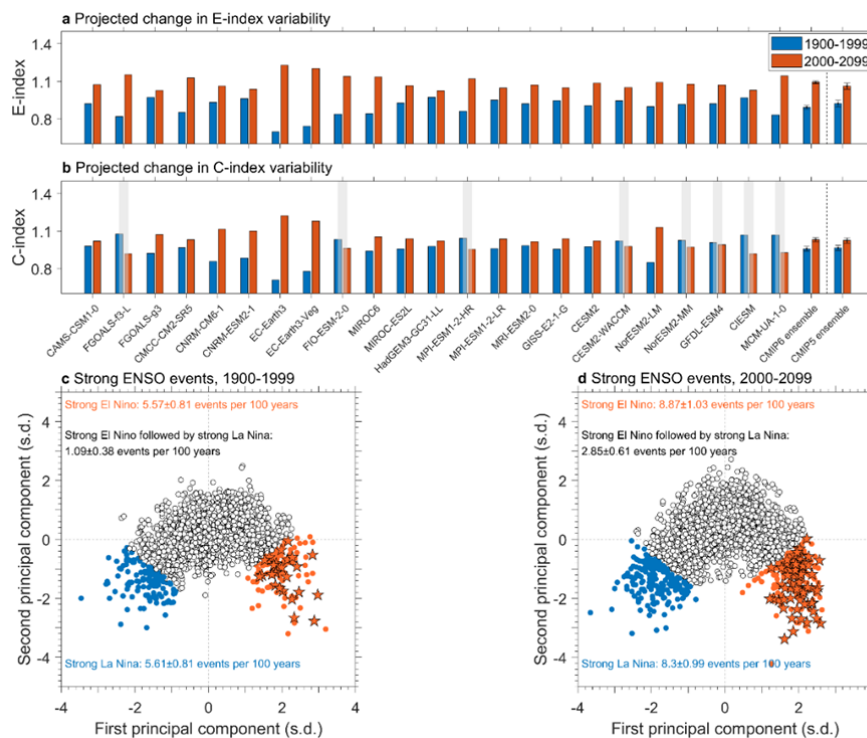
713

714

715 **Figure 3 | Observed and simulated tropical Pacific mean state and change.** a, 1980-2010 trends
 716 for reanalysis SST^{68,69,70} and surface winds^{71,72,73}. a, As in b, but for the average over 28 CMIP5 and

717 23 CMIP6 models. These models are forced by historical forcing and the representative concentration
 718 pathway 8.5 (RCP8.5) emission scenario, or the equivalent, the shared socioeconomic pathway 5-8.5
 719 (SSP5-8.5). **c**, Average SST trends over 28 CMIP5 and 23 CMIP6 models for the 1980-2009. **d**,
 720 CMIP5 and CMIP6 mean SST and surface wind bias relative to the observations for the 1980-2010
 721 period. Stippling and black contour indicate the 90% and 95% confidence levels respectively using a
 722 two-tailed *t*-test. **e**, Linear trend values over the 1980-2019 period of December-February (DJF) zonal
 723 SST gradient and eastern Pacific meridional SST gradient for the 51 CMIP 5/6 models (stars), and
 724 three reanalysis datasets^{68,69,70} (colour filled circles). Zonal SST gradient is defined following REF.⁸¹
 725 except sign-reversed, that is, the eastern Pacific (5°S-5°N, 180°E-80°W) area average SST is
 726 subtracted from the western Pacific (5°S-5°N, 110°E-180°E) area average SST. The eastern Pacific
 727 meridional SST gradient is defined as the areal average off-equatorial northern SST (5°N-10°N,
 728 90°W-150°W) and the southern SST (5°S-10°S, 150°W-90°W) minus the equatorial SST (2.5°S-
 729 2.5°N, 90°W-150°W). **f**, As in **e**, for the 2020-2100 period in the CMIP5/6 models. **Models suffers**
 730 **from a cold tongue bias and the observed trend over the past decades is within the inter-model range**
 731 **of trends over the same period, but opposite to the long-term trend in majority of models.**

732

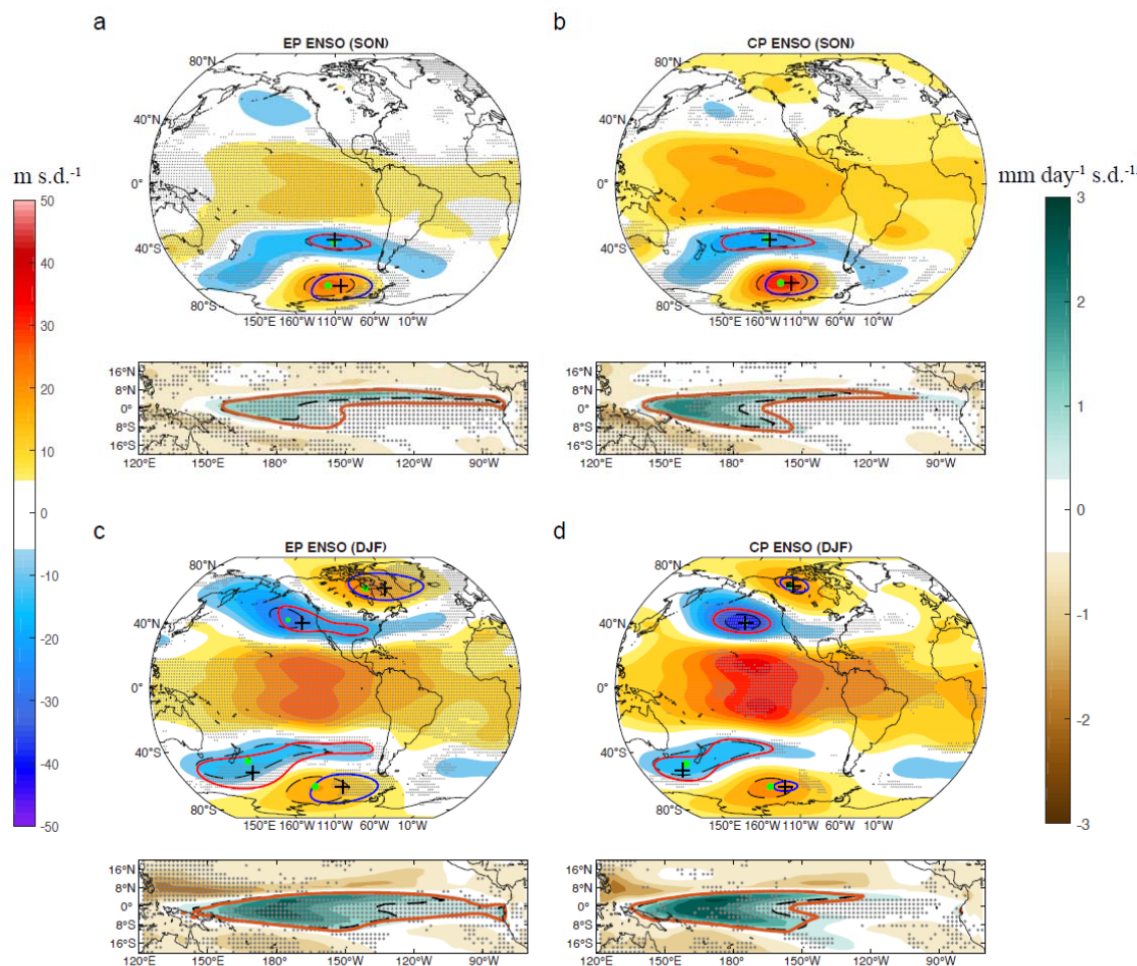


733

734

735 **Figure 4 | Projected increase in ENSO SST variability in CMIP6 models.** Shown are from 23
 736 CMIP6 models selected based on their ability to simulate ENSO nonlinearity at least 50% of the
 737 observed, as indicated by the nonlinear relationship between the first and second principal
 738 components of SST variability in the tropical Pacific²⁹. These models are forced by historical forcing
 739 up to 2014 and thereafter the shared socioeconomic pathway 5-8.5 (SSP5-8.5), the equivalent to the
 740 representative concentration pathway 8.5 (RCP8.5) emission scenario. **a**, DJF E-index standard
 741 deviation over the present day (1900-1999) and future (2000-2099) periods. All models project
 742 increased EP-ENSO variance. **b**, As in **a** but for the C-index. Models simulating a variance reduction

743 are greyed out. The multi-model mean for the CMIP6 models, and 17 CMIP5 models using in REF.²⁹
 744 are shown in a and b, with error bars indicating one standard deviation value of 10,000 realizations in
 745 a Bootstrap test. c, Relationship between the first and second principal component for identification of
 746 extreme ENSO events. Orange dots indicate extreme El Niño events (E-index > 1.5 s.d.), and blue
 747 dots indicate extreme La Niña events (C-index <= -1.75 s.d.). Orange pentagrams indicate extreme
 748 El Niño events followed by an extreme La Niña event the following year. The corresponding
 749 average frequency is labelled in each panel with 90% confidence interval based on a Poisson
 750 distribution. A stronger inter-model consensus on increased ENSO SST variability emerges in CMIP6
 751 than CMIP5 models.
 752



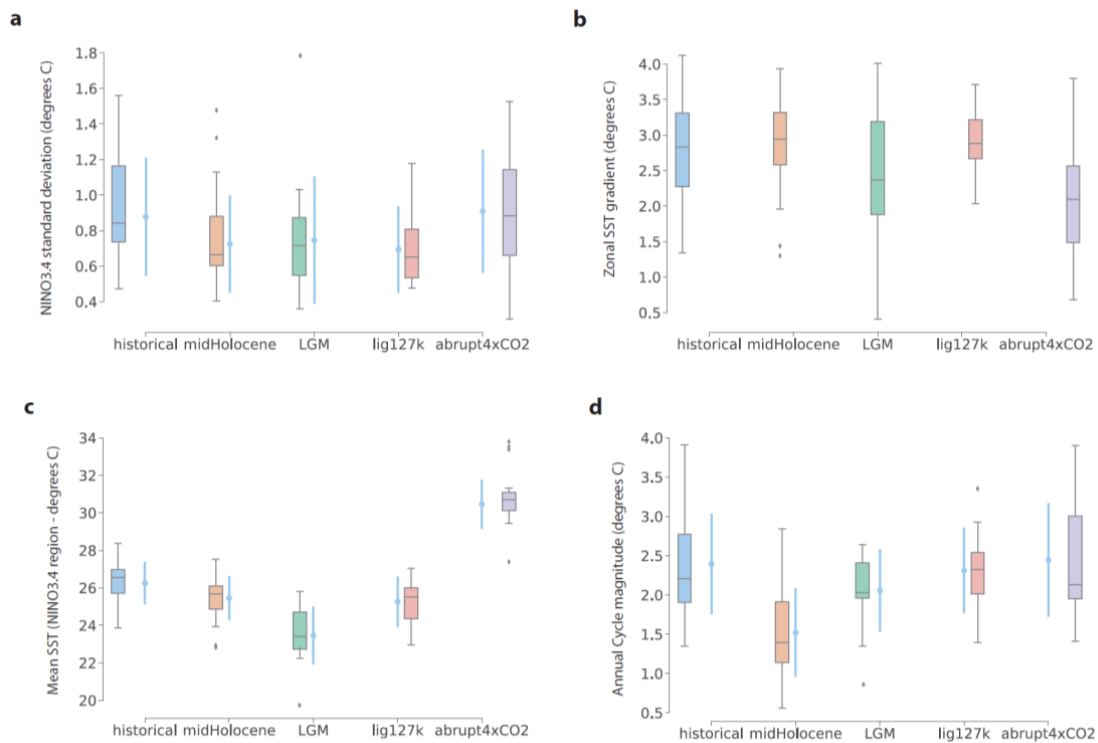
753

754 **Figure 5 | Changing ENSO teleconnections under greenhouse warming.** The results are based on
 755 CMIP6 models forced by historical forcing up to 2014 and thereafter the shared socioeconomic
 756 pathway 5-8.5 (SSP5-8.5) emission scenario. Shown are simultaneous regressions of quadratically
 757 detrended 200hPa geopotential height (m s.d.⁻¹) and rainfall anomalies (mm day⁻¹ s.d.⁻¹) onto a, b,
 758 normalized E-index and C-index for SON, and c, d, for DJF. Regression coefficients for the present-
 759 day period (1900-1999) are shaded in colour. The centres of the PSA or the PNA (upper part of each
 760 panel) for the present-day climate are indicated by a dashed contour surrounding a green dot, and
 761 for the future climate a solid contour of the same value surrounding a cross for each centre; the 1 mm
 762 day⁻¹ s.d.⁻¹ rainfall anomalies (lower part of each panel) is plotted in black dashed contour for the

763 **present-day** and **solid red** for the **future** (2000-2099) period. Results are for SON and DJF when the
 764 PSA and PNA peaks, respectively. Stippling indicates an inter-model consensus with more than two
 765 thirds of models showing same-signed response. The PSA and PNA centres during EP-ENSO are
 766 situated more to the east than during CP-ENSO, and these centres tend to either strengthen or shift
 767 eastward under greenhouse warming, particularly in the ENSO mature season of DJF.

768

769

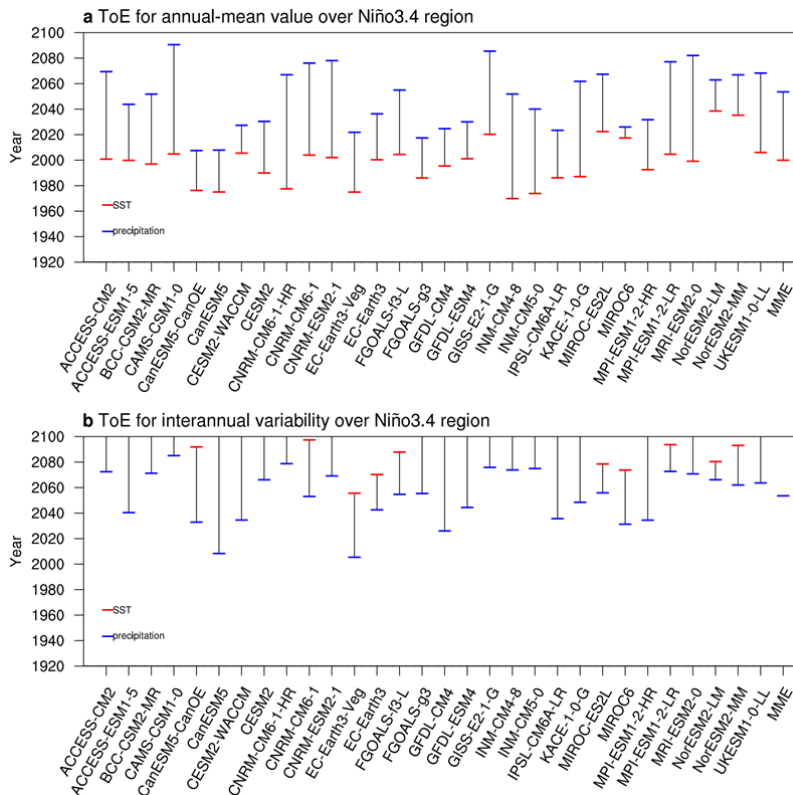


770

771 **Figure 6 | Tropical Pacific mean state and ENSO variability in past climate.** Shown are
 772 simulations with PMIP3/CMIP5 and PMIP4/CMIP6 models as described in REF.¹⁰⁵: historical, mid-
 773 Holocene, Last Glacial Maximum (LGM), last interglacial (lig127k) and abrupt 4xCO2 for **a**, Niño3.4
 774 variability, **b**, west-minus-east SST gradient, **c**, mean SST, and **d**, annual cycle magnitude in the
 775 Niño3.4 region. All the paleoclimate simulation outputs have been calendar-adjusted using the
 776 PaleoCalAdjust tool²¹⁰. The magnitude of the annual cycle is defined as the range of monthly
 777 climatological SST in the Niño3 region (5°S-5°N, 150°W-90°W), and the zonal SST gradient as the
 778 West (5°S-5°N, 100°E-180°E) minus East Pacific (5°S-5°N, 160°W-80°W) annual mean SST
 779 difference. **Boxplots** indicate **intermodel** spread, and **light blue** pointplots indicate the **spread when**
 780 **including internal variability** estimated using 100 random 50-yr samples from each model simulation
 781 (error bars draw the standard deviation of samples). **While models agree on lower ENSO variance in**
 782 **past climates than the present-day climate, its relationship with the annual cycle, zonal SST gradient**
 783 **and mean SST in the central and eastern Pacific shows vast diversity in the strength and direction.**

784

785



786

787 **Figure 7 | Time of emergence (ToE) of climate change signals.** Signals are sought from outputs of
 788 each CMIP6 model under historical forcing and shared socioeconomic pathway 5-8.5 (SSP5-8.5)
 789 emission scenario over the 1850 to 2099 period (150 years), and “noise” is diagnosed from a 500-year
 790 pre-industrial (piControl) experiment of the respective model as the standard deviation of annual-
 791 mean values. **a**, ToE for annual-mean **SST** in **Red** and **rainfall** in **blue**, both averaged over the
 792 Niño3.4 region, is provided as year when signals emerge from noise, for each model and for the
 793 multi-model ensemble (MME) mean. To obtain evolution of the signal, we regress timeseries of 150
 794 annual mean values in each grid point onto a smoothed version of the tropical-mean (30°S-30°N) by
 795 fitting a fourth-order polynomial²⁰⁶. ToE is defined as the year when the signal-to-noise ratio exceeds
 796 1. **b**, ToE for interannual variability is given as the end year of a 30-year window over which running
 797 standard deviation of annual mean anomalies is calculated. Evolution of the signal is obtained by
 798 regressing time series of 30-year running standard deviation of anomalies quadratically detrended for
 799 each 30-year period onto time series of 30-year running climatology of the tropical mean similarly
 800 smoothed by fitting a fourth-order polynomial. For illustration, ToE for interannual variability is
 801 defined as when the signal-to-noise ratio exceeds 1.5. **The ToE for interannual rainfall variability is**
 802 **sooner than that for interannual SST variability, whereas the ToE for the annual-mean rainfall is later**
 803 **than annual-mean SST.**

804

805

806 **References**

807 1. Philander, S. G. H., Yamagata, T., & Pacanowski, R. C. Unstable air-sea interactions in the
 808 tropics. *J. Atmos.* **41**, 604–613 (1984).
 809 2. Ropelewski, C. F. & Halpert, M. S. Global and regional scale precipitation patterns

- 810 associated with the El Niño/Southern Oscillation. *Mon. Wea. Rev.* **115**, 1606–1626
811 (1987).
- 812 3. McPhaden, M. J., Zebiak, S. E., & Glantz, M. H. ENSO as an integrating concept in
813 earth science. *Science*, **314**, 1740-1745 (2006).
- 814 4. L’Heureux, M. L. et al. Observing and predicting the 2015/16 El Niño. *Bull. Am.*
815 *Meteorol. Soc.* **98**, 1363–1382 (2017).
- 816 5. Santoso, A., McPhaden, M. J., & Cai, W. The defining characteristics of ENSO
817 extremes and the strong 2015/16 El Niño. *Rev. Geophys.* **55**, 1079-1129 (2017).
- 818 6. Bjerknes, J. Atmospheric teleconnections from the equatorial Pacific. *Mon. Weather*
819 *Rev.* **97**, 163-172 (1969).
- 820 7. Cai, W. et al. Climate impacts of the El Niño-Southern Oscillation on South America.
821 *Nature reviews earth & environment* **1**, 215-231 (2020).
- 822 8. Ashok, K., Behera, S. K., Rao, S. A., Weng, H. Y. & Yamagata, T. El Niño Modoki
823 and its possible teleconnection. *J. Geophys. Res.* **112**, C11007 (2007).
- 824 **Defines a type of El Niño with maximum SST anomaly in the equatorial central**
825 **Pacific atmospheric teleconnection different from El Niño with anomaly centre in**
826 **the equatorial eastern Pacific.**
- 827 9. McPhaden, M. J., Santoso, A., & Cai, W. (Eds.). El Niño Southern Oscillation in a
828 Changing Climate **253**, *John Wiley & Sons* (2020).
- 829 10. IPCC (2013). Climate Change 2013: The Physical Science Basis. Contribution of
830 Working Group I to the Fifth Assessment Report of the Intergovernmental Panel on
831 Climate Change [Stocker, T.F., Qin, D., Plattner, G.-K., Tignor, M., Allen, S.K.,
832 Boschung, J., et al. (eds.)]. Cambridge University Press, Cambridge, United Kingdom
833 and New York, NY, USA, 1535 pp
- 834 11. IPCC (2018). Global Warming of 1.5°C. An IPCC Special Report on the impacts of
835 global warming of 1.5°C above pre-industrial levels and related global greenhouse gas
836 emission pathways, in the context of strengthening the global response to the threat of
837 climate change, sustainable development, and efforts to eradicate poverty [Masson-
838 Delmotte, V., Zhai, P., Pörtner, H.-O., Roberts, D., Skea, J., Shukla, P.R., et al. (eds.)].
839 Available from <https://www.ipcc.ch/sr15/>
- 840 12. Collins, M., et al. The impact of global warming on the tropical Pacific Ocean and El
841 Niño. *Nat. Geosci.* **3**, 391-397 (2010).
- 842 13. Cai, W. et al. ENSO and Greenhouse Warming. *Nat. Clim. Change* **5**, 849–859 (2015).
- 843 14. Jin, F.-F., & Neelin, J. D. Modes of interannual tropical ocean - atmosphere
844 interaction—A unified view. Part I: Numerical results. *J. Atmos.* **50**, 3477–3503 (1993).
- 845 15. An, S.-I., & Jin, F.-F. An eigen analysis of the interdecadal changes in the structure and
846 frequency of ENSO mode. *Geophys. Res. Lett.* **27**, 1573–1576 (2000).
- 847 16. Fedorov, A. V., & Philander, S. G. A stability analysis of tropical ocean-atmosphere
848 interactions: Bridging measurements and theory for El Niño. *J. Climate* **14**, 3086–3101
849 (2001).
- 850 17. Meehl, G. A., Branstator, G. W., & Washington, W. M. Tropical Pacific interannual
851 variability and CO2 climate change. *J. Clim.* **6**, 42–63 (1993).

- 852 18. Tett, S. Simulation of El Niño - Southern Oscillation - like variability in a global
853 AOGCM and its response to CO2 increase. *J. Clim.* **8**, 1473–1502 (1995).
- 854 19. Power, S. B., Delage, F., Chung, C., Kociuba, G., & Keay, K. Robust twenty-first
855 century projections of El Niño and related precipitation variability. *Nature* **502**, 541–
856 545 (2013).
- 857 20. Yun, K. S. et al. Increasing ENSO–rainfall variability due to changes in future tropical
858 temperature–rainfall relationship. *Commun. Earth Environ.* **2**, 43 (2021).
- 859 21. Cai, W. et al. Increasing frequency of extreme El Niño events due to greenhouse
860 warming. *Nat. Clim. Change* **4**, 111–116 (2014).
- 861 22. Wang, G. et al. Continued increase of extreme El Niño frequency long after 1.5C
862 warming stabilization. *Nat. Clim. Change* **7**, 568–572 (2017).
- 863 **Finds that extreme El Niño frequency continues to increase for up to a century**
864 **after global warming is halted at 1.5°C above pre-industrial level**
- 865 23. Cai, W. et al. More extreme swings of the South Pacific convergence zone due to
866 greenhouse warming. *Nature* **488**, 365–369 (2012).
- 867 24. Santoso, A. et al. Late-twentieth-century emergence of the El Niño propagation
868 asymmetry and future projections. *Nature* **504**, 126 (2013).
- 869 25. Cai, W. et al. Increased frequency of extreme La Niña events under greenhouse
870 warming. *Nat. Clim. Change* **5**, 132–137 (2015).
- 871 26. Cobb, K. M. et al. Highly Variable El Niño-Southern Oscillation Throughout the
872 Holocene. *Science* **339**, 67-70 (2013).
- 873 27. McGregor, S., Timmermann, A. & Timm, O. A unified proxy for ENSO and PDO
874 variability since 1650. *Clim. Past* **6**, 1-17 (2010).
- 875 28. McGregor, H. et al. A weak El Niño/Southern Oscillation with delayed seasonal
876 growth around 4300 years ago, *Nat. Geosci.* **6**, 949–953 (2013).
- 877 29. Cai, W. et al. Increased variability of eastern Pacific El Niño under greenhouse
878 warming. *Nature* **564**, 201–206 (2018).
- 879 30. Luo, J.-J., Wang, G., & Dommenges, D. May common model biases reduce CMIP5’s
880 ability to simulate the recent Pacific La Niña-like cooling? *Clim. Dyn.* **18**, 1-17 (2018).
- 881 **Proposes the hypothesis that common model biases may favor an El Niño-like**
882 **warming in response to greenhouse gas forcing in CMIP5.**
- 883 31. Coats, S., & Karnauskas, K. B. A Role for the Equatorial Undercurrent in the Ocean
884 Dynamical Thermostat, *J. Clim.* **31**, 6245-6261 (2018).
- 885 32. Seager, R. et al. Strengthening tropical Pacific zonal sea surface temperature gradient
886 consistent with rising greenhouse gases. *Nat. Clim. Chang.* **9**, 517–522 (2019).
- 887 33. Chung, E. S. et al. Reconciling opposing Walker circulation trends in observations and
888 model projections. *Nat. Clim. Chang.* **9**, 405–412 (2019).
- 889 **Using satellite observations, shows a substantially less strengthening of the Pacific**
890 **Walker circulation during recent decades in satellite observations than in**
891 **reanalysis products, and a dominant role of internal variability in the**
892 **strengthening.**
- 893 34. Cai, W. et al. Pantropical climate interactions. *Science* **363**, eaav4236 (2019).

- 894 35. Cai, W., Ng, B., Geng, T., Wu, L., Santoso, A., & McPhaden, M. J. Butterfly effect and
895 a self-modulating El Niño response to global warming. *Nature* **585**, 68-73 (2020).
896 **Demonstrates that ENSO exhibits a self-regulating behaviour such that ENSO's**
897 **future variability is shaped by its past, thus modulating the effect of greenhouse**
898 **forcing.**
- 899 36. Maher, N., Matei, D., Milinski, S., & Marotzke, J. ENSO change in climate projections:
900 forced response or internal variability? *Geophys. Res. Lett.* **45**, 11-390 (2018).
- 901 37. Zheng, X.-T., Hui, C., & Yeh, S. W. Response of ENSO amplitude to global warming
902 in CESM large ensemble: uncertainty due to internal variability. *Clim. Dyn.* **50**, 4019-
903 4035 (2018).
- 904 38. Ng, B., Cai, W., Cowan, T., & Bi, D. (2021). Impacts of Low-Frequency Internal
905 Climate Variability and Greenhouse Warming on El Niño–Southern Oscillation, *J.*
906 *Clim.* **34**, 2205-2218 (2021).
- 907 39. Eyring, V. et al. Overview of the Coupled Model Intercomparison Project Phase 6
908 (CMIP6) experimental design and organization. *Geosci. Model Dev.* **9**, 1937–1958
909 (2016).
- 910 40. Fu, C. & Fletcher, J. O. Two patterns of equatorial warming associated with El Niño.
911 *Mon. Sci. J.* **30**, 1360-1364 (In Chinese) (1985).
912 **Shows that there are two types of equatorial warming associated with El Niño.**
- 913 41. Fu, C., Diaz, H. F. & Fletcher, J. O. Characteristics of the response of sea surface
914 temperature in the central Pacific associated with warm episodes of the Southern
915 Oscillation. *Mon. Wea. Rev.* **114**, 1716-1738 (1986).
- 916 42. Capotondi, A. et al. Understanding ENSO diversity. *Bull. Am. Meteorol. Soc.* **96**, 921–
917 938 (2015).
- 918 43. Capotondi, A., Wittenberg, A.T., Kug, J.-S., Takahashi, K., & McPhaden, M. J. ENSO
919 Diversity. [ENSO in a Changing Climate: Challenges, Paleo-Perspectives, and](#)
920 [Outlook.](#) *In El Niño Southern Oscillation in a Changing Climate (eds M.J. McPhaden,*
921 *A. Santoso and W. Cai).* AGU Monograph, (2020)
- 922 44. Takahashi, K., & Dewitte, B. Strong and moderate nonlinear El Niño regimes. *Clim.*
923 *Dyn.* **46**, 1627–1645 (2016).
- 924 45. Timmermann, A. et al. (2018). El Niño-southern oscillation complexity. *Nature* **559**,
925 535-545.
- 926 46. Dommenges, D., Bayr, T., & Frauen, C. Analysis of the non-linearity in the pattern and
927 time evolution of El Niño Southern Oscillation. *Clim. Dyn.* **40**, 2825-2847 (2013).
- 928 47. Takahashi, K., Montecinos, A., Goubanova, K., & Dewitte, B. ENSO regimes:
929 Reinterpreting the canonical and Modoki El Niño. *Geophys. Res. Lett.* **38**, L10704
930 (2011).
- 931 48. Karamperidou, C., Jin, F.-F. & Conroy, J. L. The importance of ENSO nonlinearities in
932 tropical Pacific response to external forcing. *Clim. Dyn.* **49**, 2695–2704 (2017).
- 933 49. Lee, T., & McPhaden, M. J. Increasing intensity of El Niño in the central-equatorial
934 Pacific. *Geophys. Res. Lett.* **37**, L14603 (2010).

- 935 50. Capotondi, A., & Sardeshmukh, P. D. Is El Niño really changing? *Geophys. Res. Lett.*
936 **44**, 8548–8556 (2017).
- 937 51. Wang, B. *et al.* Historical change of El Niño properties sheds light on future changes of
938 extreme El Niño. *Proc. Natl. Acad. Sci.* **116**, 22512-17 (2019).
- 939 52. Zhang, Q., Guan, Y. & Yang, H. ENSO amplitude change in observation and coupled
940 models. *Adv. Atmos. Sci.* **25**, 361–366 (2008).
- 941 53. Kim, S. T. *et al.* Response of El Niño sea surface temperature variability to greenhouse
942 warming. *Nat. Clim. Chang.* **4**, 786–790 (2014).
- 943 54. Geng, T., Cai, W., & Wu, L. Two types of ENSO varying in tandem facilitated by
944 nonlinear atmospheric convection. *Geophys. Res. Lett.* **47**, e2020GL088784 (2020).
- 945 55. Kennedy, J. J. A review of uncertainty in in situ measurements and data sets of sea
946 surface temperature. *Reviews of Geophysics* **52**, 1-32 (2014).
- 947 56. Li, J. *et al.* El Niño modulations over the past seven centuries. *Nat. Clim. Change* **3**,
948 822-826 (2013).
- 949 57. Liu, Y. *et al.* Recent enhancement of central Pacific El Niño variability relative to last
950 eight centuries. *Nat. Commun.* **8**, 15386 (2017).
- 951 58. Grothe, P. R. *et al.* Enhanced El Niño–Southern oscillation variability in recent decades,
952 *Geophys. Res. Lett.* **47**, e2019GL083906 (2020)
- 953 **Shows decreased ENSO variance 3-5,000 years ago and ENSO strengthening in**
954 **the last five decades, using a new ensemble of fossil coral oxygen isotope records**
955 **from the central equatorial Pacific.**
- 956 59. Karamperidou, C. *et al.* [ENSO in a Changing Climate: Challenges, Paleo-Perspectives,](#)
957 [and Outlook.](#) *In El Niño Southern Oscillation in a Changing Climate (eds M.J.*
958 *McPhaden, A. Santoso and W. Cai).* AGU Monograph, (2020).
- 959 60. Freund, M. *et al.* Higher frequency of Central Pacific El Niño events in recent decades
960 relative to past centuries, *Nat. Geosci.* **12**, 450-455 (2019)
- 961 61. Philip, S. Y. & van Oldenborgh, G. J. Shifts in ENSO coupling processes under global
962 warming. *Geophys. Res. Letts.* **33**, L11704 (2006).
- 963 62. Jin, F.-F., Kim, S. T. & Bejarano, L. A coupled-stability index for ENSO. *Geophys.*
964 *Res. Lett.* **33**, L23708. (2006).
- 965 63. Kim, S. T., & Jin, F.-F. An ENSO stability analysis. Part II: Results from the twentieth
966 and twenty-first century simulations of the CMIP3 models. *Clim. Dyn.* **36**, 1609-1627
967 (2011).
- 968 64. Carréric, A. *et al.* Change in strong Eastern Pacific El Niño events dynamics in the
969 warming climate. *Clim. Dyn.* **54**, 901 (2020).
- 970 65. Dewitte, B., Yeh, S.-W., Moon, B.-K., Cibot, C., & Terray, L. Rectification of the
971 ENSO variability by interdecadal changes in the equatorial background mean state in a
972 CGCM simulation. *J. Clim.* **20**, 2002-2021 (2007).
- 973 66. Timmermann, A. *et al.* Increased El Niño frequency in a climate model forced by
974 future greenhouse warming. *Nature* **398**, 694–697 (1999).
- 975 67. Thual, S., Dewitte, B., An, S.-I., & Ayoub, N. Sensitivity of ENSO to stratification in a
976 recharge-discharge conceptual model. *J. Clim.* **4**, 4331-4348 (2011).

- 977 **Refines theoretical framework showing intensified ocean-atmosphere coupling as**
978 **the mean upper-ocean stratification increases.**
- 979 68. Rayner, N. A. et al. Global analyses of sea surface temperature, sea ice, and night
980 marine air temperature since the late nineteenth century, *J. Geophys. Res.* **108**, 4407
981 (2003).
- 982 69. Huang, B. et al. Extended Reconstructed Sea Surface Temperature version 5
983 (ERSSTv5), Upgrades, validations, and intercomparisons. *J. Clim.*, **30**, 8179–8205
984 (2017).
- 985 70. Ishii, M., A. Shouji, S. Sugimoto, & T. Matsumoto. Objective Analyses of Sea-Surface
986 Temperature and Marine Meteorological Variables for the 20th Century using
987 ICOADS and the Kobe Collection. *Int. J. Climatol.* **25**, 865-879 (2005).
- 988 71. Slivinski, L. C. et al. Towards a more reliable historical reanalysis: Improvements for
989 version 3 of the Twentieth Century Reanalysis system. *Quart. J. R. Meteorol. Soc.* **145**,
990 2876-2908 (2019).
- 991 72. Poli, P. et al. ERA-20C: An atmospheric reanalysis of the twentieth century. *J. Clim.*
992 **29**, 4083-4097 (2016).
- 993 73. Kobayashi, S. et al. The JRA-55 Reanalysis: General specifications and basic
994 characteristics. *J. Meteorol. Soc. Japan Ser. II.* **93**, 5-48 (2015).
- 995 74. Lian, T., Chen, D., Ying, J., Huang, P. & Tang, Y. Tropical Pacific trends under global
996 warming: El Niño-like or La Niña-like? *Natl. Sci. Rev.* **5**, 810-812 (2018).
- 997 75. Cai, W., et al. ENSO Response to Greenhouse Forcing. *In El Niño Southern Oscillation*
998 *in a Changing Climate (eds M.J. McPhaden, A. Santoso and W. Cai), AGU*
999 *Monograph*, (2020).
- 1000 76. Knutson, T. R., & Manabe, S. Time-Mean Response over the Tropical Pacific to
1001 Increased CO₂ in a Coupled Ocean-Atmosphere Model, *J. Clim.* **8**, 2181-2199 (1995).
- 1002 77. Liu, Z., Vavrus, S., He, F., Wen, N., & Zhong, Y. Rethinking Tropical Ocean Response
1003 to Global Warming: The Enhanced Equatorial Warming, *J. Clim.* **18**, 4684-4700
1004 (2005).
- 1005 78. Xie, S., Deser, C., Vecchi, G. A., Ma, J., Teng, H., & Wittenberg, A. T. Global
1006 Warming Pattern Formation: Sea Surface Temperature and Rainfall, *J. Clim.* **23**, 966-
1007 986 (2010).
- 1008 79. Meehl, G. & Washington, W. El Niño-like climate change in a model with increased
1009 atmospheric CO₂ concentrations. *Nature* **382**, 56–60 (1996).
- 1010 80. Clement, A. C., Seager, R., Cane, M. A., & Zebiak, S. E. An Ocean Dynamical
1011 Thermostat, *J. Clim.* **9**, 2190-2196 (1996).
- 1012 81. Watanabe, M. et al. Enhanced warming constrained by past trends in equatorial Pacific
1013 sea surface temperature gradient. *Nat. Clim. Chang.* **11**, 33–37 (2021).
- 1014 82. Kociuba, G., & Power, S. B. Inability of CMIP5 Models to Simulate Recent
1015 Strengthening of the Walker Circulation: Implications for Projections, *J. Clim.* **28**, 20-
1016 35 (2015).
- 1017 83. Coats, S., & Karnauskas, K. B. Are simulated and observed twentieth century tropical
1018 Pacific sea surface temperature trends significant relative to internal

- 1019 variability? *Geophys. Res. Lett.* **44**, 9928– 9937 (2017).
- 1020 84. Zhang, L. et al. Indian Ocean warming trend reduces Pacific warming response to
1021 anthropogenic greenhouse gases: An interbasin thermostat mechanism. *Geophys. Res.*
1022 *Lett.* **46**, 10882-10890 (2019).
- 1023 85. McGregor, S. et al. Recent Walker circulation strengthening and Pacific cooling
1024 amplified by Atlantic warming. *Nat. Clim. Change* **4**, 888–892 (2014).
- 1025 86. Meehl, G.A. et al. Atlantic and Pacific tropics connected by mutually interactive
1026 decadal-timescale processes. *Nat. Geosci.* **14**, 36–42 (2021).
- 1027 87. Li, X., Xie, S.-P., Gille, S. T., & Yoo, C. Atlantic induced pan-tropical climate change
1028 over the past three decades. *Nat. Clim. Change* **6**, 275–279 (2016).
- 1029 88. Lee, S.-K., Kim, D., Foltz, G. R., & Lopez, H. Pantropical response to global warming
1030 and the emergence of a La Niña-like mean state trend. *Geophys. Res. Lett.* **47**,
1031 e2019GL086497 (2020).
- 1032 89. McGregor, S. et al. Model tropical Atlantic biases underpin diminished Pacific decadal
1033 variability. *Nat. Clim. Change* **8**, 493–498 (2018).
- 1034 90. Kajtar, J. B., Santoso, A., McGregor, S., England, M. H., & Baillie, Z. Model under-
1035 representation of decadal Pacific trade wind trends and its link to tropical Atlantic bias.
1036 *Clim. Dyn.* **50**, 1471–1484 (2018).
- 1037 91. Li, C., Dommenges, D. & McGregor, S. Trans-basin Atlantic-Pacific connections
1038 further weakened by common model Pacific mean SST biases. *Nat. Commun.* **11**, 5677
1039 (2020).
- 1040 92. Stuecker, M. F. et al. Strong remote control of future equatorial warming by off-
1041 equatorial forcing. *Nat. Clim. Chang.* **10**, 124–129 (2020).
- 1042 **Demonstrates opposite signed feedbacks in the equatorial and off equatorial**
1043 **regions to greenhouse gas forcing via coupled interactions between clouds, Hadley**
1044 **Circulation, and oceanic subtropical cells.**
- 1045 93. Heede, U. K., Fedorov, A. V., & Burls, N. J. Time Scales and Mechanisms for the
1046 Tropical Pacific Response to Global Warming: A Tug of War between the Ocean
1047 Thermostat and Weaker Walker, *J. Clim.* **33**, 6101-6118 (2020).
- 1048 94. Cai, W., & Whetton, P. H. Evidence for a time - varying pattern of greenhouse
1049 warming in the Pacific Ocean. *Geophys. Res. Lett.* **27**, 2577-2580 (2000).
- 1050 95. Zheng, X.-T., Xie, S.-P., Lv, L. H., & Zhou, Z. Q. Intermodel uncertainty in ENSO
1051 amplitude change tied to Pacific Ocean warming pattern. *J. Clim.* **29**, 7265–7279
1052 (2016).
- 1053 96. Kohyama, T., Hartmann, D. L., & Battisti, D. S. La Niña–like Mean-State Response to
1054 Global Warming and Potential Oceanic Roles, *J. Clim.* **30**, 4207-4225 (2017).
- 1055 97. Hayashi, M., Jin, F.-F. & Stuecker, M. F. Dynamics for El Niño-La Niña asymmetry
1056 constrain equatorial-Pacific warming pattern. *Nat. Commun.* **11**, 4230 (2020).
- 1057 98. Ying, J., Huang, P., Lian, T., & Tan, H. Understanding the effect of an excessive cold
1058 tongue bias on projecting the tropical Pacific SST warming pattern in CMIP5 models.
1059 *Clim. Dyn.* **52**, 1805–1818 (2018).
- 1060 99. Taschetto, A. S., Sen Gupta, A., Jourdain, N., Santoso, A., Ummerhofer, C. C., &

- 1061 England, M. H. Cold tongue and warm pool ENSO events in CMIP5: mean state and
1062 future projections. *J. Clim.* **27**, 2861–2885 (2014).
- 1063 100.Philip, S. Y. & van Oldenborgh, G. J. Shifts in ENSO coupling processes under global
1064 warming. *Geophys. Res. Letts.* **33**, L11704 (2006).
- 1065 101.DiNezio, P. N., Kirtman, B. P., Clement, A. C., Lee, S.-K., Vecchi, G. A., &
1066 Wittenberg, A. Mean climate controls on the simulated response of ENSO to increasing
1067 greenhouse gases. *J. Clim.* **25**, 7399–7420 (2012).
- 1068 102.Dommenget, D., & Vijayeta, A. Simulated future changes in ENSO dynamics in the
1069 framework of the linear recharge oscillator model. *Clim. Dyn.* **53**, 4233–4248 (2019).
- 1070 103.Chen, C., Cane, M. A., Wittenberg, A. T., & Chen, D. ENSO in the CMIP5 simulations:
1071 Life cycles, diversity, and responses to climate change. *J. Clim.* **30**, 775–801 (2017).
- 1072 104.Wang, G., Cai, W., & Santoso, A. Stronger increase in the frequency of extreme
1073 convective El Niño than extreme warm El Niño under greenhouse warming. *J. Clim.* **33**,
1074 675-690 (2020).
- 1075 105.Brown, J. R. et al. Comparison of past and future simulations of ENSO in
1076 CMIP5/PMIP3 and CMIP6/PMIP4 models. *Clim. Past* **16**, 1777–1805 (2020).
- 1077 106.Zheng, X.-T., Hui, C., Xie, S.-P., Cai, W. & Long, S.-M. Intensification of El Niño
1078 rainfall variability over the tropical Pacific in the slow oceanic response to global
1079 warming. *Geophys. Res. Lett.* **46**, 2253-2260 (2019).
- 1080 107.Feng, J., Lian, T., Ying, J., Li, J. & Li, G. Do CMIP5 models show El Niño diversity?
1081 *J. Clim.*, **33**, 1619-1641 (2020).
- 1082 108.Lemmon, D. E. & Karnauskas, K. B. A Metric for Quantifying ENSO Diversity with
1083 Implications for ENSO–Mean State Interaction. *Clim. Dyn.*, **52**, 7511-7523. doi:
1084 10.1007/s00382-018-4194-3 (2019).
- 1085 109.Fredriksen, H.-B., Berner, J., Subramanian, A. C., & Capotondi, A. How does El Niño-
1086 Southern Oscillation change under global warming-A first look at CMIP6. *Geophys.*
1087 *Res. Lett.* **47**, e2020GL090640 (2020).
- 1088 110.Planton, Y. et al. Evaluating Climate Models with the CLIVAR 2020 ENSO Metrics
1089 Package. *Bull. Am. Meteorol. Soc.* **102**, E193-E217 (2021).
- 1090 111.McKenna, S., Santoso, A., Sen Gupta, A., Taschetto, A., & Cai, W. Indian Ocean
1091 Dipole in CMIP5 and CMIP6: Characteristics, biases, and links to ENSO. *Sci. Rep.* **10**,
1092 11500 (2020).
- 1093 112.Zelinka, M. D. et al. Causes of higher climate sensitivity in CMIP6 models. *Geophys.*
1094 *Res. Lett.* **47**, e2019GL085782 (2020).
- 1095 113.Zhou, Z.-Q., Xie, S.-P., Zheng, X.-T., Liu, Q. & Wang, H. Global warming-induced
1096 changes in El Niño teleconnections over the North Pacific and North America. *J. Clim.*
1097 **27**, 9050–9064 (2014).
- 1098 114.Bonfils, C. J. et al. Relative contributions of mean-state shifts and ENSO-driven
1099 variability to precipitation changes in a warming climate. *J. Clim.* **28**, 9997–10013.
1100 (2015).
- 1101 115.Huang P. Time-varying response of ENSO-induced tropical Pacific rainfall to global
1102 warming in CMIP5 models. Part II: intermodel uncertainty. *J. Clim.* **30**, 595–608 (2017).

- 1103 116.Chen, Z., Gan, B., Wu, L. & Jia, F. Pacific-North American teleconnection and North
1104 Pacific Oscillation: historical simulation and future projection in CMIP5 models. *Clim.*
1105 *Dyn.* **50**, 4379–4403 (2018).
- 1106 117.Yeh, S.-W. et al. Atmospheric teleconnections and their response to greenhouse gas
1107 forcing. *Rev Geophys.* **56**, 185–206 (2018).
- 1108 118.Michel, C., Li, C., Simpson, I. R., Bethke, I., King, M. P. & Sobolowski, S. The
1109 Change in the ENSO Teleconnection under a Low Global Warming Scenario and the
1110 Uncertainty due to Internal Variability. *J. Clim.* **33**, 4871-4889 (2020).
- 1111 119.Sohn, B.-J., Yeh, S.-W., Lee, A. & Lau, W. K. M. Regulation of atmospheric
1112 circulation controlling the tropical Pacific precipitation change in response to CO₂
1113 increases. *Nat. Commun.* **10**, 1-8 (2018).
- 1114 120.Yan, Z., Wu, B., Li, T., Collins, M., Clark, R., Zhou, T., Murphy, J. & Tan, G.
1115 Eastward Shift and Extension of ENSO-Induced Tropical Precipitation Anomalies
1116 under Global Warming. *Sci. Adv.* **6**, eaax4177 (2020).
- 1117 121.Stevenson, S. L., Significant changes to ENSO strength and impacts in the twenty-first
1118 century: Results from CMIP5. *Geophys. Res. Lett.* **39**, L17703 (2012).
- 1119 122.Tedeschi, R. G. & Collins, M. The influence of ENSO on South American precipitation:
1120 simulation and projection in CMIP5 models. *Int. J. Climatol.* **37**, 3319–3339 (2017).
- 1121 123.Power, S. B. & Delage, F. P. D. El Niño–Southern Oscillation and Associated Climatic
1122 Conditions around the World during the Latter Half of the Twenty-First Century. *J.*
1123 *Clim.* **31**, 6189–6207 (2018).
- 1124 124.Perry, S. J., McGregor, S., Sen Gupta, A., England, M. H. Future changes to El Niño-
1125 Southern Oscillation temperature and precipitation teleconnections. *Geophys. Res. Lett.*
1126 **44**,10608–10616 (2017).
- 1127 125.Lyon, B. The strength of El Niño and the spatial extent of tropical drought. *Geophys.*
1128 *Res. Lett.*, **3**, L21204 (2004).
- 1129 126.Delage, F.P.D. & Power, S.B. The impact of global warming and the El Niño-Southern
1130 Oscillation on seasonal precipitation extremes in Australia. *Clim. Dyn.* **54**, 4367–4377
1131 (2020).
- 1132 127.Lin, I.-I. et al. ENSO and Tropical Cyclones. *In El Niño Southern Oscillation in a*
1133 *Changing Climate (eds M.J. McPhaden, A. Santoso and W. Cai). AGU Monograph,*
1134 (2020).
- 1135 128.Chand, S. et al. Projected increase in El Niño-driven tropical cyclone frequency in the
1136 Pacific. *Nat. Clim. Change* **7**, 123–127 (2017).
- 1137 **Shows that during future climate ENSO, tropical cyclones become more frequent**
1138 **during El Niño and less frequent during La Niña over the off-equatorial western**
1139 **Pacific and central North Pacific islands.**
- 1140 129.Ying, J., Huang, P., Lian, T. & Chen, D. Intermodel Uncertainty in the Change of
1141 ENSO’s Amplitude under Global Warming: Role of the Response of Atmospheric
1142 Circulation to SST Anomalies. *J. Clim.* **32**, 369-383 (2019).
- 1143 130.Rodríguez-Fonseca, B. et al. Are Atlantic Niños enhancing Pacific ENSO events in
1144 recent decades? *Geophys. Res. Lett.* **36**, L20705 (2009).

- 1145 131.Ding, H., Keenlyside, N. S., & Latif, M. Impact of the equatorial Atlantic on the El
1146 Niño Southern Oscillation. *Clim. Dyn.* **38**, 1965-1972 (2012).
- 1147 132.Ham, Y.-G., Kug, J.-S., Park, J.-Y., & Jin, F.-F. Sea surface temperature in the north
1148 tropical Atlantic as a trigger for El Niño/Southern Oscillation events. *Nat. Geosci.* **6**,
1149 112–116 (2013).
- 1150 133.Kug, J.-S., & Kang, I.-S. Interactive feedback between ENSO and the Indian Ocean. *J.*
1151 *Clim.* **19**, 1784–1801 (2006).
- 1152 134.Cai, W., Sullivan, A., & Cowan, T. Interactions of ENSO, the IOD, and the SAM in
1153 CMIP3 models. *J. Clim.* **24**, 1688-1704 (2011).
- 1154 135.Kucharski, F., Syed, F. S., Burhan, A., Farah, I., & Gohar, A. Tropical Atlantic
1155 influence on Pacific variability and mean state in the twentieth century in observations
1156 and CMIP5. *Clim. Dyn.* **44**, 881–896 (2015).
- 1157 136.Choi, J. Y., Ham, Y. G., & McGregor, S. Atlantic-Pacific SST Gradient Change
1158 Responsible for the Weakening of North Tropical Atlantic-ENSO Relationship due to
1159 Global Warming. *Geophys. Res. Lett.* **46**, 7574-7582 (2019).
- 1160 137.Jia, F., Wu, L., Gan, B., & Cai, W. Global warming attenuates the tropical Atlantic-
1161 Pacific teleconnection. *Sci. Rep.* **6**, 20078 (2016).
- 1162 138.Jia, F. et al. Weakening Atlantic Niño-Pacific connection under greenhouse warming.
1163 *Sci. Adv.* **5**, eaax4111 (2019).
- 1164 139.Kug, J.-S., Vialard, J., Ham, Y.-G., Yu, J.-Y. & Lengaigne, M. ENSO Remote Forcing.
1165 *In El Niño Southern Oscillation in a Changing Climate (eds M.J. McPhaden, A.*
1166 *Santoso and W. Cai). AGU Monograph, (2020)*
- 1167 140.Cheng, W., Chiang, J. C. H., & Zhang, D. Atlantic Meridional Overturning Circulation
1168 (AMOC) in CMIP5 Models: RCP and Historical Simulations, *J. Clim.* **26**, 7187-7197
1169 (2013).
- 1170 141.Park, J. H. et al. Effect of recent Atlantic warming in strengthening Atlantic–Pacific
1171 teleconnection on interannual timescale via enhanced connection with the Pacific
1172 meridional mode. *Clim. Dyn.* **53**, 371–387 (2019).
- 1173 142.Wang, L., Yu, J.-Y. & Paek, H. Enhanced biennial variability in the Pacific due to
1174 Atlantic capacitor effect. *Nat. Commun.* **8**, 14887 (2017).
- 1175 143.Le, T., & Bae, D.-H. Causal links on interannual timescale between ENSO and the IOD
1176 in CMIP5 future simulations. *Geophys. Res. Lett.* **46**, 2820–2828 (2019).
- 1177 144.Sun, D.-Z., et al. Radiative and dynamical feedbacks over the equatorial cold tongue:
1178 results from nine atmospheric GCMs. *J. Clim.* **19**, 4059–4074 (2006).
- 1179 145.Lloyd, J., Guilyardi, E., Weller, H. & Slingo, J. The role of atmosphere feedbacks
1180 during ENSO in the CMIP3 models. *Atmos. Sci. Lett.* **10**, 170–176 (2009).
- 1181 146.Beobide-Arsuaga, G. et al. Uncertainty of ENSO-amplitude projections in CMIP5 and
1182 CMIP6 models. *Clim. Dyn.*, 1-14 (2021).
- 1183 147.Guilyardi, E., Capotondi, A., Lengaigne, M., Thual, S. & Wittenberg, A. T. ENSO
1184 Modeling. *In El Niño Southern Oscillation in a Changing Climate (eds M.J. McPhaden,*
1185 *A. Santoso and W. Cai). AGU Monograph, (2020)*

- 1186 148. Bellenger, H., Guilyardi, E., Leloup, J. Lengaigne, M., & Vialard, J. ENSO
1187 representation in climate models: From CMIP3 to CMIP5. *Clim. Dyn.* **42**, 1999–2018
1188 (2014).
- 1189 149. Kim, S.-T., Cai, W., Jin, F.-F., & Yu, J.-Y. ENSO stability in coupled climate models
1190 and its association with mean state. *Clim. Dyn.* **42**, 3313–3321 (2014).
- 1191 150. Bayr, T., Wengel, C., Latif, M., Dommenges, D., Lübbecke, J., & Park, W. Error
1192 compensation of ENSO atmospheric feedbacks in climate models and its influence on
1193 simulated ENSO dynamics. *Clim. Dyn.* **53**, 155–172 (2019)
- 1194 151. Watanabe, T. et al., Permanent El Niño during the Pliocene warm period not supported
1195 by coral evidence. *Nature* **471**, 209–211 (2011).
- 1196 152. White, S. M., & Ravelo, A. C.. Dampened El Niño in the early Pliocene warm
1197 period. *Geophys. Res. Lett.* **47**, e2019GL085504 (2020).
- 1198 153. Fedorov, A. et al. The Pliocene paradox (mechanisms for a permanent El
1199 Niño), *Science* **312** 1485–1489 (2006).
- 1200 154. Steph, S., et al. Early Pliocene increase in thermohaline overturning: A precondition
1201 for the development of the modern equatorial Pacific cold
1202 tongue, *Paleoceanography*, **25**, PA2202 (2010).
- 1203 155. Manucharyan, G. E. & Fedorov, A. V. Robust ENSO across a Wide Range of Climates,
1204 *J. Clim.* **27**, 5836-5850 (2014).
- 1205 156. Ford, H. L., A. C. Ravelo, & P. J. Polissar. Reduced El Niño–Southern Oscillation
1206 during the Last Glacial Maximum. *Science* **347**, 255–258 (2015).
- 1207 157. Koutavas, A. & S. Joanides El Niño–Southern Oscillation extrema in the Holocene and
1208 Last Glacial Maximum, *Paleoceanography* **27**, PA4208 (2012).
- 1209 158. Rustic, G. T., Koutavas, A., Marchitto, T. M. & Linsley, B. K. Dynamical excitation
1210 of the tropical Pacific Ocean and ENSO variability by Little Ice Age cooling. *Science*
1211 **350**, 1537–1541 (2015).
- 1212 159. Sadekov, A., Ganeshram, R., Pichevin, L., Berdin, R., McClymont, E., Elderfield,
1213 H. & Tudhope, A. W. Palaeoclimate reconstructions reveal a strong link between El
1214 Niño–Southern Oscillation and tropical Pacific mean state. *Nat. Commun.* **4**, 2692
1215 (2013).
- 1216 160. Glaubke, R. H., Thirumalai, K., Schmidt, M. W. & Hertzberg, J. E. Discerning
1217 Changes in High-Frequency Climate Variability Using Geochemical Populations of
1218 Individual Foraminifera, *Paleoceanogr. Paleoclimatol.* **36**, (2021).
- 1219 161. Wyman, D. A., Conroy, J. L., & Karamperidou, C. The Tropical Pacific ENSO–Mean
1220 State Relationship in Climate Models over the Last Millennium, *J. Clim.* **33**, 7539-
1221 7551 (2020).
- 1222 162. Timmermann, A., & Jin, F. F. A nonlinear mechanism for decadal El Niño amplitude
1223 changes. *Geophys. Res. Lett.* **29**, 3-1 (2002).
- 1224 163. Hayashi, M. & Jin, F. F. Subsurface nonlinear dynamical heating and ENSO
1225 asymmetry. *Geophys. Res. Lett.* **44**, 12-427 (2017).
- 1226 164. Conroy, J., J. T. Overpeck, & J. E. Cole El Niño/Southern Oscillation and changes in
1227 the zonal gradient of tropical Pacific sea surface temperature over the last 1.2

- 1228 ka. *PAGES News* **18**, 32–34 (2010).
- 1229 165. Rustic, G. T., Polissar, P. J., Ravelo, A. C., & White, S. M. Modulation of late
1230 Pleistocene ENSO strength by the tropical Pacific thermocline, *Nat. Commun.* **11**, 5377
1231 (2020).
- 1232 166. Liu, Z. Y. et al. Evolution and forcing mechanisms of El Niño over the past 21,000
1233 years. *Nature* **515**, 550–553 (2014).
- 1234 167. Karamperidou, C., Di Nezio, P. N., Timmermann, A., Jin, F.-F. & Cobb, K. M. The
1235 response of ENSO flavors to mid-Holocene climate: Implications for proxy
1236 interpretation. *Paleoceanography* **30**, 527 (2015).
- 1237 168. Chen, L., Zheng, W. & Braconnot, P. Towards understanding the suppressed ENSO
1238 activity during mid-Holocene in PMIP2 and PMIP3 simulations. *Clim. Dyn.* **53**, 1095–
1239 1110 (2019).
- 1240 169. Masson-Delmotte, V. et al. Information from paleo-climate archives. *Climate Change*
1241 *2013: The Physical Science Basis (eds. T. F. Stocker et al.)*, Cambridge University
1242 Press, 383–464 (2013).
- 1243 170. Tudhope, A. W. et al. Variability in the El Niño–Southern oscillation through a glacial-
1244 interglacial cycle, *Science* **291**, 1511–1517 (2001).
- 1245 171. Emile-Geay, J. Links between tropical Pacific seasonal, interannual and orbital
1246 variability during the Holocene, *Nat. Geosci.* **9**, 168–173 (2016)
- 1247 172. Carré, M. et al. Holocene history of ENSO variance and asymmetry in the eastern
1248 tropical Pacific. *Science* **345**, 1045 (2014).
- 1249 173. White, S. M., Ravelo, A. C. & Polissar, P. J. Dampened El Niño in the early and mid-
1250 Holocene due to insolation-forced warming/deepening of the thermocline, *Geophys.*
1251 *Res. Lett.* **45**, doi: 10.1002/2017GL075433 (2018).
- 1252 174. Rodbell, D. T., Seltzer, G. O., Anderson, D. M., Abbott, M. B., Enfield, D. B. &
1253 Newman, J. H. An ~15,000 year record of El Niño-driven alluviation in southwestern
1254 Ecuador, *Science* **283**, 516–520 (1999).
- 1255 175. Moy, C. M., G. O. Seltzer, D. T. Rodbell, & D. M. Anderson Variability of El Niño-
1256 Southern Oscillation activity at millennial timescales during the Holocene epoch,
1257 *Nature* **420**, 162–165 (2002).
- 1258 176. Conroy, J. L., Overpeck, J. T., Cole, J. E., Shanahan, T. M. & Steinitz-Kannan, M.
1259 Holocene changes in eastern tropical Pacific climate inferred from a Galápagos lake
1260 sediment record, *Quat. Sci. Rev.* **27**, 1166–1180 (2008).
- 1261 177. Zhang, Z., Leduc, G. & Sachs, J. P. El Niño evolution during the Holocene revealed
1262 by a biomarker rain gauge in the Galápagos Islands, *Earth Planet. Sci. Lett.* **404**, 420-
1263 434 (2014).
- 1264 178. Chen, S., Hoffmann, S. S., Lund, D. C., Cobb, K. M., Emile-Geay, J. & Adkins, J. F.
1265 A high-resolution speleothem record of western equatorial Pacific rainfall: Implications
1266 for Holocene ENSO evolution, *Earth Planet. Sci. Lett.* **442**, 61–71 (2016).
- 1267 179. Karamperidou, C. et al. ENSO diversity and teleconnections in the Holocene: the
1268 impact of Eastern, Central and Coastal El Niño in proxy-critical locations, submitted
1269 (2021)
- 1270 180. McGregor, S., Khodri, M., Maher, N., Ohba, M., Pausata, F. S. R., & Stevenson, S.

- 1271 The effect of strong volcanic eruptions on ENSO. *In El Niño Southern Oscillation in a*
1272 *Changing Climate (eds M.J. McPhaden, A. Santoso and W. Cai). AGU Monograph,*
1273 (2020)
- 1274 181.Adams, J. B., Mann, M. E. & Ammann, C. M. Proxy evidence for an El Niño-like
1275 response to volcanic forcing. *Nature* **426**, 274-278 (2003).
- 1276 182.Emile-Geay, J., Seager, R., Cane, M. A., Cook, E. R., & Haug, G. H. Volcanoes and
1277 ENSO over the Past Millennium, *J. Clim.* **21**, 3134-3148 (2008).
- 1278 183.Ohba, M., Shiogama, H., Yokohata, T. & Watanabe, M. Impact of strong tropical
1279 volcanic eruptions on ENSO simulated in a coupled GCM, *J. Clim.* **26**, 5169–5182
1280 (2013).
- 1281 184.Stevenson, S., Otto-Bliesner, B., Fasullo, J., & Brady, E. “El Niño like” hydroclimate
1282 responses to last millennium volcanic eruptions. *J. Clim.* **29**, 2907-2921 (2016).
- 1283 185.Khodri, M. et al., Tropical explosive volcanic eruptions can trigger El Niño by cooling
1284 tropical Africa, *Nat. Commun.* **8**, 1-13 (2017).
- 1285 186.McGregor, S. & Timmermann, A. The Effect of Explosive Tropical Volcanism on
1286 ENSO. *J. Clim.* **24**, 2178-2191 (2011).
- 1287 187.Zanchettin, D. et al. Bidecadal variability excited in the coupled ocean–atmosphere
1288 system by strong tropical volcanic eruptions. *Clim. Dyn.* **39**, 419–444 (2012).
- 1289 188.Robock, A. Volcanic eruptions and climate, *Rev. Geophys.* **38**, 191–219 (2000).
- 1290 189.Ding, Y., J. A. Carton, G. A. Chepurin, G. Stenchikov, A. Robock, L. T. Sentman, & J.
1291 P. Krasting, Ocean response to volcanic eruptions in Coupled Model Intercomparison
1292 Project 5 (CMIP5) simulations, *J. Geophys. Res. Oceans.* **119**, 5622–5637 (2014).
- 1293 190.Dee, S. G. et al. No consistent ENSO response to volcanic forcing over the last
1294 millennium. *Science* **367**, 1477–1481 (2020).
- 1295 **Shows that proxy records reveal an insignificant tendency for an El Niño-like**
1296 **response in the year after a strong volcanic eruption, at odds with the strong**
1297 **tendencies found in climate models.**
- 1298 191.Pausata, F. S. R., Karamperidou, C., Caballero, R., & Battisti, D. S. ENSO response to
1299 high-latitude volcanic eruptions in the northern hemisphere: The role of the initial
1300 conditions. *Geophys. Res. Lett.* **43**, 8694-8702 (2016).
- 1301 192.Stevenson, S., Fasullo, J. T., Otto-Bliesner, B. L., Tomas, R. A., & Gao, C. Role of
1302 eruption season in reconciling model and proxy responses to tropical volcanism. *Proc.*
1303 *Natl. Acad. Sci.* **114**, 1822–1826 (2017).
- 1304 193.Zanchettin, D. et al. Clarifying the relative role of forcing uncertainties and initial-
1305 condition unknowns in spreading the climate response to volcanic eruptions. *Geophys.*
1306 *Res. Lett.* **46**, 1602–1611 (2019).
- 1307 194.Pausata, F. S. R., Zanchettin, D., Karamperidou, C., Caballero, R., & Battisti, D. S.
1308 ITCZ shift and extratropical teleconnections drive ENSO response to volcanic eruptions.
1309 *Sci. Adv.* **6**, eaaz5006 (2020)
- 1310 195.Predybaylo, E. et al. El Niño/Southern Oscillation response to low-latitude volcanic
1311 eruptions depends on ocean pre-conditions and eruption timing. *Commun Earth*
1312 *Environ* **1**, 1-13 (2020)

- 1313 196.Emile-Geay, J., & Tingley, M. Inferring climate variability from nonlinear proxies:
1314 application to palaeo-enso studies. *Clim. Past* **12**, 31–50 (2016).
1315 **Demonstrates the pitfalls of ignoring nonlinearities in the proxy–climate**
1316 **relationship, which often exaggerates climate variability changes inferred by**
1317 **proxies and leads to reconstructions with poorly quantified uncertainties.**
- 1318 197.Kiefer, J., & Karamperidou, C. High-resolution modeling of enso-induced precipitation
1319 in the tropical andes: Implications for proxy interpretation. *Paleoceanogr.*
1320 *Paleoclimatol.* **34**, 217-236 (2019).
- 1321 198.Dee, S., Okumura, Y., Stevenson, S., & Di Nezio, P. Enhanced North American ENSO
1322 Teleconnections During the Little Ice Age Revealed by Paleoclimate Data Assimilation.
1323 *Geophys. Res. Lett.* **47**, e2020GL087504 (2020).
- 1324 199.Chang, P. et al. Pacific meridional mode and El Niño-Southern Oscillation. *Geophys.*
1325 *Res. Lett.* **34**, L16608 (2007).
- 1326 200.Vimont, D. J., Alexander, M. & Fontaine, A. Midlatitude excitation of tropical
1327 variability in the Pacific: The role of thermodynamic coupling and seasonality. *J. Clim.*
1328 **22**, 518-534 (2009).
- 1329 [201.Stuecker, M. F. Revisiting the Pacific Meridional Mode, *Sci. Rep.* **8**, 1-9 \(2018\).](#)
- 1330 202.Hong, L. C., & Jin, F. F. A southern hemisphere booster of super El Niño. *Geophys.*
1331 *Res. Lett.* **41**, 2142-2149 (2014).
- 1332 203.Holmes, R. M., McGregor, S., Santoso, A. & England, M. H. Contribution of Tropical
1333 Instability Waves to ENSO Irregularity. *Clim. Dyn.* **52**, 1837-1855 (2019).
- 1334 204.Bony, S. & Dufresne, J. L. Marine boundary layer clouds at the heart of tropical cloud
1335 feedback uncertainties in climate models. *Geophys. Res. Lett.* **32**, L20806 (2005).
- 1336 205.Deser, C. et al. Insights from Earth system model initial-condition large ensembles and
1337 future prospects. *Nat. Clim. Change* **10**, 277–286 (2020)
- 1338 206.Hawkins, E. & Sutton, R. Time of emergence of climate signals. *Geophys. Res. Lett.* **39**,
1339 L01702 (2012).
- 1340 207.Jochum, M. & Murtugudde, R. Temperature advection by tropical instability waves. *J.*
1341 *Phys. Oceanogr.* **36**, 592-605 (2006).
- 1342 208.An, S. I. Interannual Variations of the Tropical Ocean Instability Wave and ENSO. *J.*
1343 *Clim.* **21**, 3680-3686 (2008).
- 1344 209.Chu, J.-E. et al. Reduced tropical cyclone densities and ocean effects due to
1345 anthropogenic greenhouse warming. *Sci. Adv.* **6**, eabd5109 (2020).
- 1346 210.Bartlein, P. J. & Shafer, S. L. Paleo calendar-effect adjustments in time-slice and
1347 transient climate-model simulations (PaleoCalAdjust v1.0): impact and strategies for
1348 data analysis, *Geosci. Model Dev.* **12**, 3889–3913 (2019).
- 1349

1350 Acknowledgements

1351 This work is supported by the Strategic Priority Research Program of Chinese Academy of
1352 Sciences, Grant No. XDB40000000. W.C., A.S., B.N., and G.W. are supported by Centre for
1353 Southern Hemisphere Oceans Research (CSHOR) a joint research facility between QNLM

1354 and CSIRO (CSHOR). We acknowledge the World Climate Research Programme, which,
1355 through its Working Group on Coupled Modelling, coordinated and promoted CMIP6. We
1356 thank the climate modelling groups for producing and making available their model output,
1357 the Earth System Grid Federation (ESGF) for archiving the data and providing access, and
1358 the multiple funding agencies who support CMIP6 and ESGF. PMIP is endorsed by both
1359 WCRP/WGCM and Future Earth/PAGES. MFS was supported by NOAA's Climate Program
1360 Office's Modeling, Analysis, Predictions, and Projections (MAPP) program grant
1361 NA20OAR4310445 and participates in the MAPP Marine Ecosystem Task Force. This is
1362 PMEL contribution number 5213. M.L. is supported by the ARISE ANR (Agence Nationale
1363 pour la Recherche) project (ANR-18-CE01-0012). Xiaopei L. is supported by the National
1364 Natural Science Foundation of China (41925025 and 92058203). B.G. was supported by the
1365 National Natural Science Foundation of China (41922039). A.C. is supported by the NOAA
1366 Climate Program Office Climate Variability and Predictability (CVP), and Modeling,
1367 Analysis, Predictions and Projections (MAPP) Programs. M.C. was supported by NERC
1368 grant NE/S004645/1. This is IPRC publication 1525 and SOEST contribution 11356. A.S.T.
1369 is supported by the Australian Research Council (ARC FT160100495). S.-W.Y. is funded by
1370 the Korean Meteorological Administration Research and Development Program under grant
1371 (KMI2020-01213). Y.Y. is supported by the National Natural Science Foundation of China
1372 (NSFC) project (grant no. 41976005). Xichen L. is supported by National Key R&D Program
1373 of China (2018YFA0605703) and the National Natural Science Foundation of China (Grants
1374 41976193). M.C. is supported by NERC grant NE/S004645/1. T.B. is funded by Deutsche
1375 Forschungs Gemeinschaft (DFG) project "Influence of Model Bias on ENSO Projections of
1376 the 21st Century" through grant 429334714. C.K. is supported by US NSF Award AGS-
1377 1902970. J.R.B. acknowledges support from the ARC Centre of Excellence for Climate
1378 Extremes (CE170100023). J.Y. is supported by National Natural Science Foundation of
1379 China (Grants 41690121, 41690120). A.T. was supported by the Institute for Basic Science
1380 (IBS-R028-D1). S.M. acknowledges support from the Australian Research Council through
1381 grant number Ft160100162. J.-S.K. is supported by the National Research Foundation of
1382 Korea (NRF-2018R1A5A1024958). X.-T. Z. is funded by the National Natural Science
1383 Foundation of China (41975092). B.D. acknowledges support from Fondecyt (Grant
1384 1190276) and ANR (Grant ANR-18-CE01-0012).

1385 **Author contributions**

1386 W.C. and A.S. conceived the study. W.C., M.J.M., M.F.S., M.L., A.S., J-S.K., A.S.T., S.-W.
1387 Y., C.K., B.D., M.C., A.T. coordinated the presentation and discussion for various sections.
1388 F.J., B.N., G.W., Y.Y., J.Y. contributed to analysis and graphic of various figures. All authors
1389 contributed to the manuscript preparation, interpretation, discussion, and writing, led by W.C.

1390

1391 **Competing interests**

1392 The authors declare no competing interests.